Ore Geology Reviews 158 (2023) 105494

Contents lists available at ScienceDirect

Ore Geology Reviews

journal homepage: www.elsevier.com/locate/oregeorev

LA-ICPMS trace elements and C-O isotopes constrain the origin of the Danaopo Cd-Ge-bearing Zn-Pb deposit, western Hunan, China

Tao Wu [a], Zhilong Huang [a,*], Chen Wei [a,b], Lin Ye [a,*], Zaifei Yan [a], Zhenzhong Xiang [a,c], Yusi Hu [a], Zhiheng Sui [d]

[a] State Key Laboratory of Ore Deposit Geochemistry, Institute of Geochemistry, Chinese Academy of Sciences, Guiyang 550081, China
[b] Helmholtz-Zentrum Dresden-Rossendorf, Helmholtz Institute Freiberg for Resource Technology, Chemnitzer Str. 40, 09599 Freiberg, Germany
[c] University of Chinese Academy of Sciences, Beijing 100049, China
[d] Team 405, Bureau of Geology and Mineral Exploration and Development of Hunan Province, Jishou 416099, China

ARTICLE INFO

Keywords:
Sphalerite in-situ trace element
Critical metals
Nature of ore-forming fluid
Ore genesis
MVT deposits

ABSTRACT

The Danaopo Zn-Pb deposit, hosted in algal limestone, is the second largest Zn-Pb deposit (150 Mt ores at an average grade of 3.06% Zn + Pb) in the western Hunan-eastern Guizhou metallogenic belt (WHEGMB). Here we investigate the trace elements of sphalerite and C-O isotopes and rare earth elements (REEs) of calcite in the Danaopo deposit, aiming to present insights into the mineralization potentiality of critical metals and origin of Zn-Pb deposits in the WHEGMB. In-situ trace element reveals the inhomogeneous distribution of critical metals within sphalerite, including Cd (1520 to 11570 ppm), Ge (0.73 to 236 ppm), Ga (0.04 to 26.90 ppm), and Tl (0.01 to 3.62 ppm). Cd and Ge exceed the Chinese comprehensive utilization standard. The LA-ICPMS elemental map and inter-element correlations suggest that Cd and Ge enter sphalerite lattice via the substitution of $Zn^{2+} \leftrightarrow Cd^{2+}$ and $4Zn^{2+} \leftrightarrow Ge^{4+} + 2Fe^{2+} + \square$ (vacancy), respectively. The $\delta^{13}C_{PDB}$ (-3.93 to −0.12‰) values of the ore-stage calcite indicate that the carbon in hydrothermal fluids primarily originates from the dissolution of Cambrian algal limestone. Calculated $\delta^{18}O_{fluid}$ (+5.23 to + 9.95‰) values on calcites lies between the oxygen isotopic compositions of the algal limestone (+18.76 to + 23.87‰) and the basinal hot brine (+4 to + 10‰), implying that the oxygen was sourced from a binary mixing of ore-host rocks and basin brine. Besides, the REE distribution pattern of Cal-I falls within the field of ore-host rocks. In contrast, Cal-II is plotted between the Cambrian ore-host and Proterozoic Banxi Group to Cambrian Niutitang Formation footwall. These findings suggest that REE of Cal-I was mainly sourced from country carbonate rocks, while Cal-II has mixed REE origins from ore-host rocks and footwall sedimentary and metamorphic basement rocks. Overall, based on detailed deposit geology, sphalerite trace elements, and calcite C-O and REE evidences, this study concludes that the Danaopo is a classic Mississippi Valley-type (MVT) Zn-Pb deposit with a low-temperature and low fO_2 reductive ore-forming fluid.

1. Introduction

The world-class western Hunan-eastern Guizhou metallogenic belt (WHEGMB) is located in the southeastern Yangtze block (Fig. 1a) and contains over 300 carbonate hosted Zn-Pb deposits with a total of > 600 million tonnes (Mt) sulfide ores at an average grade of 4% Zn + Pb (Li et al., 2014; Wu et al., 2021; Hu et al., 2022). The western Hunan mining area alone has>20.0 Mt Zn-Pb metals, which can be further divided into four Zn-Pb-(Hg) orefields from north to south, including Luota (~2.0 Mt), Baojing (~1.0 Mt), Huayuan (~15.0 Mt), and Fenghuang (~2.0 Mt) (Fig. 1c; Yang and Lao, 2007; Kuang et al., 2015). The giant Zn-Pb mineralization in western Hunan was formed during the Caledonian collision orogeny (ca. 490 ~ 410 Ma; Duan et al., 2014; Yao and Li, 2016; Tan et al., 2018; Zhou et al., 2021), making it one of the most important lead and zinc production bases in China (Zhou et al., 2014). Sphalerites from these Zn-Pb deposits associated with rich endowment of critical metals including cadmium (Cd), gallium (Ga), and germanium (Ge), such as Ga-Ge enriched Luota orefield (Wu et al., 2021) and Cd-

* Corresponding authors.
E-mail addresses: wutao@mail.gyig.ac.cn (T. Wu), huangzhilong@vip.gyig.ac.cn (Z. Huang), weichen@mail.gyig.ac.cn (C. Wei), yelin@vip.gyig.ac.cn (L. Ye), yanzaifei@mail.gyig.ac.cn (Z. Yan), xiangzhenzhong@mail.gyig.ac.cn (Z. Xiang), huyusi@mail.gyig.ac.cn (Y. Hu).

https://doi.org/10.1016/j.oregeorev.2023.105494
Received 11 January 2023; Received in revised form 10 May 2023; Accepted 18 May 2023
Available online 22 May 2023

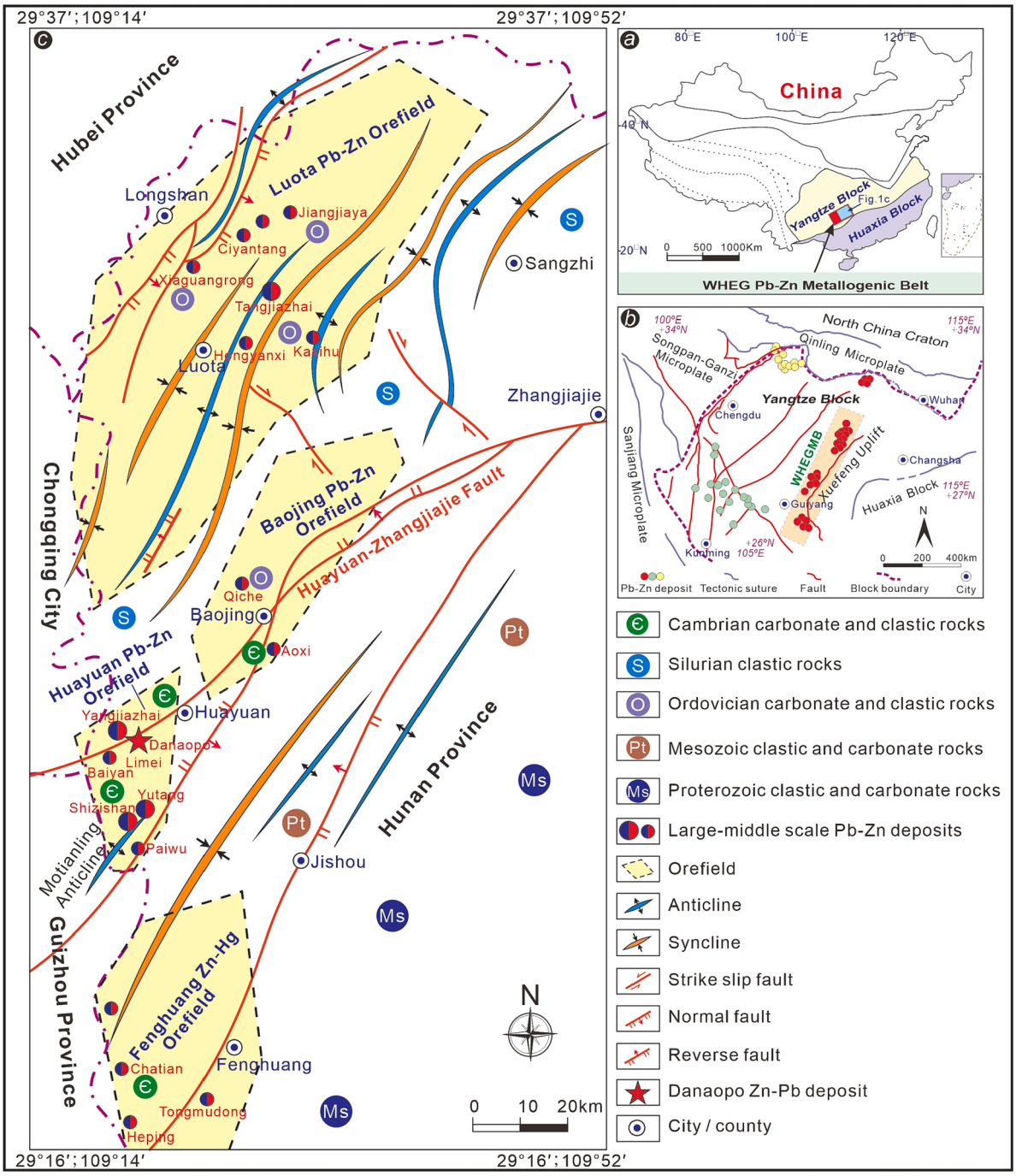

Fig. 1. (a) Tectonic map of China (modified after Zhou et al., 2013). (b) Geological sketch map of the Yangtze block (modified after Luo et al., 2020); (c) Regional geologic map of the WHEGMB, showing the distributions of strata, major structures, and Zn-Pb deposits (modified after Yang and Lao, 2007).

(Ge) enriched Huayuan orefield (Wei et al., 2021c).

Previous studies on Zn-Pb deposits at WHEGMB were focused mainly on unraveling the mineralization features, metal sources, formation age, and precipitation mechanism (Schneider et al., 2002; Duan et al., 2014; Cao et al., 2017; Zhou et al., 2018a, 2022; Hu et al., 2022 and reference therein). However, the nature of ore-forming fluids and the ore genesis of these Zn-Pb deposits are still debated. For instance, the ore genesis has been disputed as sedimentary rework type (Li, 1992), synsedimentary-type (Luo et al., 2009), or Mississippi Valley Type (MVT) (Cai et al., 2014; Hu et al., 2022). The occurrence and distribution of critical metals in western Hunan are still unclear, which has led to the neglect of the comprehensive utilization of critical metals in this area.

The Danaopo deposit is a recently discovered Cd-Ge-bearing Zn-Pb deposit with identified Zn + Pb of approximately 4.57 Mt, making it one of the largest deposits in the Huayuan orefield. The Zn-Pb orebodies are located in the algal limestone of the Lower Cambrian Qingxudong Formation (Fm) and the formation and distribution of these orebodies are primarily dominated by the Huayuan-Zhangjiajie regional fault (Wei et al., 2020). Our previous study conducted on the Danaopo deposit suggested that the reduced sulfur was sourced from thermochemical sulfate reduction (TSR) of coeval seawater sulfates in the ore host sequence. The ore lead and zinc were originated from the mixing of various metal sources, including metamorphic basement rocks of the Proterozoic Banxi Group, footwall black shale of the Lower Cambrian Niutitang Fm, and ore-host algal limestone, based on detailed geology and sulfide in-situ S-Pb isotopes (Wu et al., 2021). However, the origin of

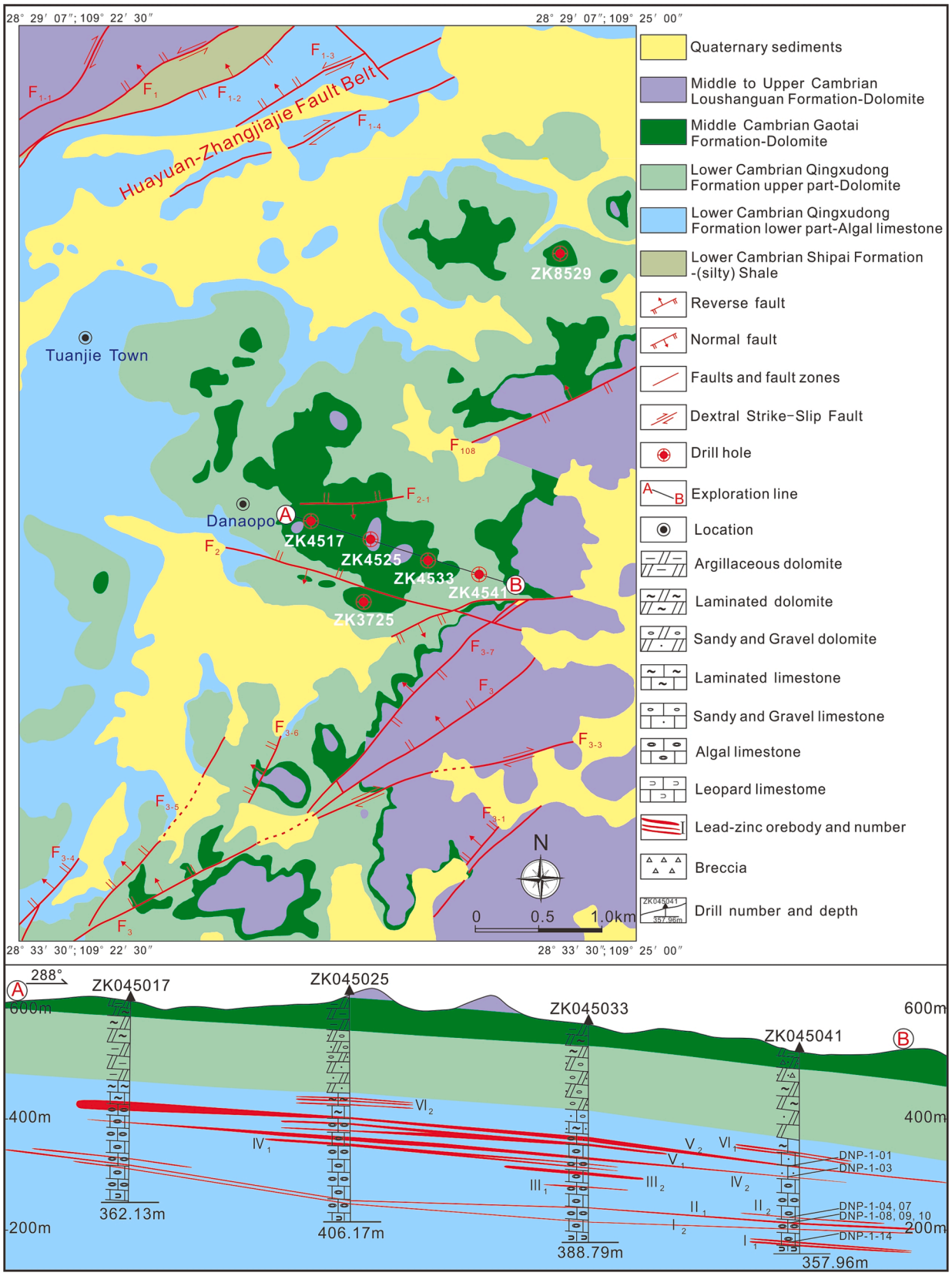

Fig. 2. Geologic map of the Danaopo deposit, showing the distributions of strata, faults, drill holes, as well as the details of cross-section of the exploration line No. 45 (modified after Yu et al., 2014; Wu et al., 2021).

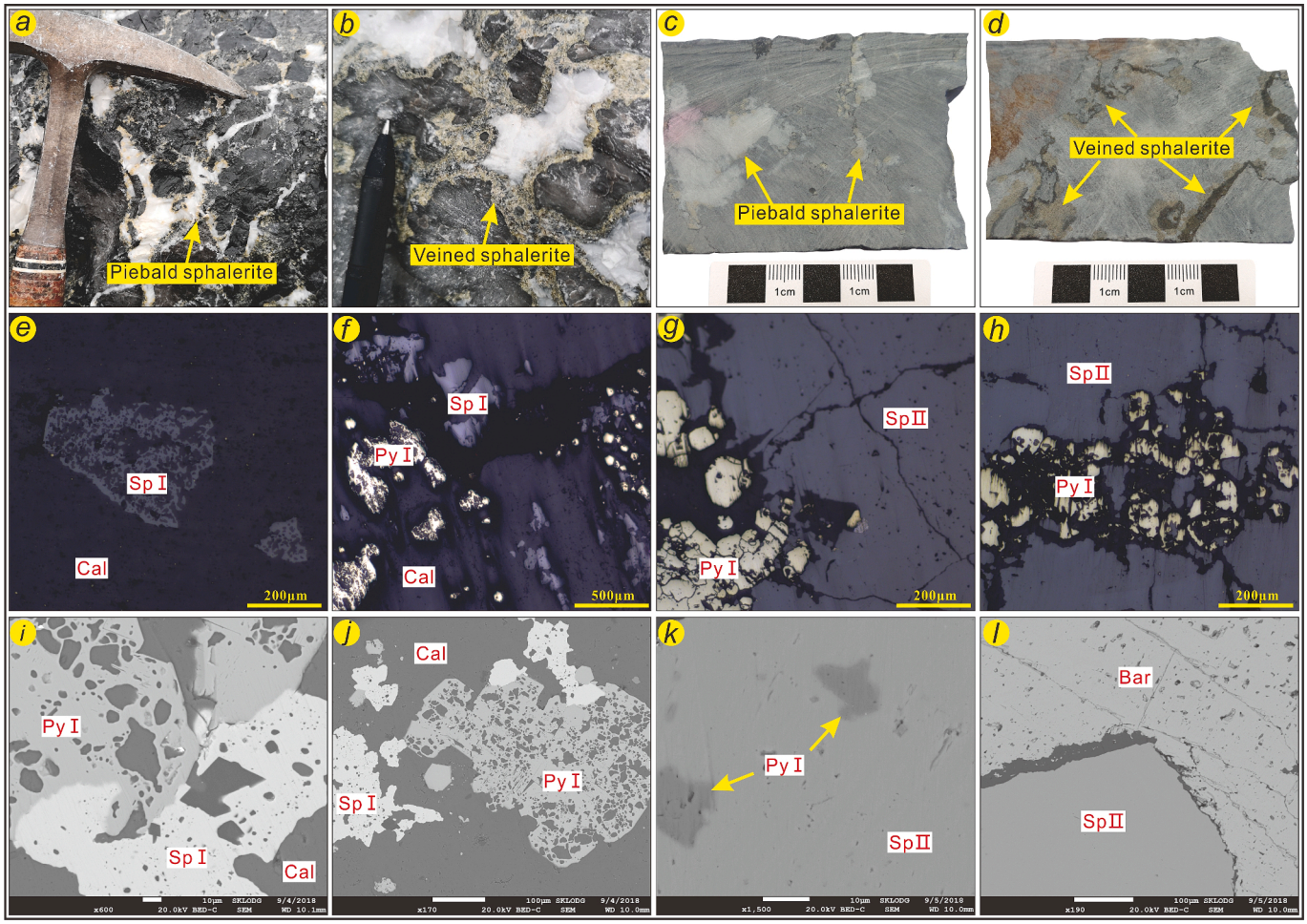

Fig. 3. Field (a-b), hand-specimen (c-d), microscope (e-h), and SEM (i-l) photographs of occurrence and textures of sulfide orebodies and ores at Danaopo: (a, c) piebald sphalerite in algal limestone; (b, d) sphalerite vein in algal limestone; (e, f, i, j) anhedral Sp-I and Py-I occur as metasomatic relict in Cal; (g, h, k) subhedral-anhedral Py-I filled and enclosed by coarse-veined Sp-II; (l) diagenetic barite replaced by coarse-veined Sp-II. Abbreviations: Py-I: pyrite in early ore-stage; Sp-II: sphalerite in main ore-stage; Cal: calcite; Bar: barite.

ore-forming fluid, the economic potential of critical metals, and the ore genesis at Danaopo remain poorly constrained.

Here, we conducted LA-ICPMS trace elements of sphalerite and calcite, as well as calcite C-O isotopes on the Danaopo deposit to trace the source of carbon, oxygen and rare earth elements (REEs) in ore-forming fluids, investigate the occurrence and distribution of critical metals in sphalerite, and determine its deposit genesis. The findings will provide further insights on understanding the origin of the Danaopo deposit and an effective basis for comprehensive utilization of critical metals in the Huayuan orefield.

2. Geological setting

The Yangtze block is an essential part of the South China block (Fig. 1a; Zhou et al., 2013), which is mainly bounded by four terranes, including the Cathaysia block to southeast, Qinling microplate to north, Songpan-Ganzi microplate to northwest, and Sanjiang microplate to west (Zhou et al., 2018c; Luo et al., 2020; Fig. 1b). The WHEGMB, adjacent to the NE-trending Xuefeng uplift, is situated in the southeastern Yangtze block (Fig. 1b). The southeastern Yangtze terrane is composed of the Meso-Neoarchean crystalline basement, Proterozoic metamorphic basement, and sedimentary covers. The crystalline basement is composed of the Kongling Group gneiss and amphibolite, the metamorphic basement is made up of the Banxi Group sandstone, silty slate and sedimentary tuff, and the sedimentary covers are composed of the Sinian to Quaternary clastic and carbonate rocks (Duan et al., 2014). Multi-stage folds and faults were formed during the Wuling, Caledonian, Hercynian and Indosinian-Yanshanian orogenic episodes and are broadly distributed in the WHEGMB (Fig. 1c; Li et al., 2014). Regional magmatism occurred in the Neoproterozoic era, but it was minor (840–503 Ma; Zhang et al., 2014; Wang et al., 2008) and unrelated to Zn-Pb mineralization (Yang and Lao, 2007).

The Danaopo Zn-Pb deposit in the northeastern Huayuan orefield is positioned in the middle of the WHEGMB (Fig. 1b and c). Exposed stratigraphy in the ore region consist mainly of the Lower Cambrian Shipai and Qingxudong Formations (Fms), as well as the Middle Cambrian Gaotai and Loushanguan Fms (Fig. 2). The Shipai Fm is primarily made up of silty shale (Fig. 2). The Qingxudong Fm, which occurs as thick to skinny bedded and normally involves algal/leopard/argillaceous/sandy/gravel limestone and argillaceous/laminated micritic dolostone, is the primary ore-host in the entire WHEGMB (Fig. 2). The Gaotai and Loushanguan Fms are composed of thick-bedded to thin argillaceous dolostone and thick-bedded laminated argillaceous dolostone, respectively (Fig. 2). The NE-, NW- and ENE-trending faults are well developed at Danaopo (Fig. 2; Mao, 2016). The NE-trending dextral strike-slip normal faults (F1-group; Fig. 2) were generated by *syn*-ore movement of the Huayuan-Zhangjiajie fault belt, which were considered as regional ore-fluid conduits (Wei et al., 2020). The F1-generated open-space structures (i.e., joints, fractures and pores) in the ore-host algal limestone provided metal deposition site for the ore-forming fluid (Fu,

Table 1
In-situ trace element composition of sphalerite at Danaopo ($\times 10^{-6}$).

Sample	Ore-stage	Location		Mn	Fe	Cu	Ga	Ge	Ag	Cd	Sn	Sb	Pb	Tl
DNP-1-14 (n = 12)	I	ZK4541	Min.	0.12	409	0.68	0.30	1.70	0.05	4220	0.11	<DL	160	0.01
		(180 m)	Max.	65.7	4110	50.7	23.8	76.2	2.05	8990	0.18	<DL	449	0.91
			Mean	10.4	1111	24.4	5.98	17.3	1.29	5756	0.15	<DL	252	0.28
			S.D.	19.0	1221	15.5	7.72	20.7	0.55	1463	0.03	<DL	82.1	0.31
DNP-2-02 (n = 9)	I	ZK3725	Min.	0.12	227	0.51	0.04	0.73	0.04	3151	0.08	<DL	163	0.01
		(416 m)	Max.	0.75	4830	28.2	25.6	6.16	1.17	9020	0.89	<DL	307	0.13
			Mean	0.38	851	8.13	3.56	2.37	0.38	5745	0.38	<DL	235	0.04
			S.D.	0.26	1499	10.6	8.91	2.54	0.46	1901	0.29	<DL	43.7	0.05
DNP-3-01 (n = 7)	I	ZK8529	Min.	0.33	349	36.7	1.64	4.56	0.27	3930	0.16	0.18	87.3	0.06
		(309 m)	Max.	70.5	690	82.5	26.9	27.6	0.68	7618	1.12	0.55	337	0.78
			Mean	23.8	494	56.6	12.6	13.7	0.48	5948	0.61	0.32	170	0.32
			S.D.	29.1	103	17.5	10.1	9.15	0.12	1155	0.39	0.20	82.3	0.29
DNP-3-08 (n = 7)	I	ZK8529	Min.	2.47	488	20.0	2.16	1.51	1.31	5040	0.47	<DL	71.2	0.17
		(234 m)	Max.	201	974	74.0	20.8	14.6	6.03	11,570	2.84	<DL	232	1.08
			Mean	105	659	42.8	10.6	6.24	3.20	7533	1.43	<DL	147	0.61
			S.D.	74.0	165	17.5	7.55	4.54	1.62	2230	0.86	<DL	54.0	0.31
(n = 35)	I		Min.	0.12	227	0.51	0.04	0.73	0.04	3151	0.08	0.18	71.2	0.00
			Max.	201	4830	82.5	26.9	76.2	6.03	11,570	2.84	0.64	449	1.08
			Mean	32.8	830	30.5	7.71	12.1	1.30	6147	0.65	0.38	210	0.31
			S.D.	54.8	1037	23.2	8.81	15.0	1.33	1777	0.66	0.20	79.0	0.32
DNP-1-04 (n = 7)	II	ZK4541	Min.	2.05	1110	2.02	0.11	15.8	0.04	1520	0.10	<DL	234	0.17
		(222 m)	Max.	183	8160	121	17.4	101	4.68	9210	1.10	<DL	338	1.23
			Mean	46.7	4204	59.8	7.68	62.0	2.35	5068	0.36	<DL	294	0.59
			S.D.	64.0	2959	43.0	5.64	39.0	1.50	3204	0.42	<DL	43.0	0.37
DNP-1-07 (n = 8)	II	ZK4541	Min.	11.0	4000	8.60	1.66	36.1	0.74	2230	0.10	<DL	235	0.36
		(220 m)	Max.	42.1	5950	17.0	5.82	116	2.31	7830	0.47	<DL	416	1.35
			Mean	20.7	5211	13.0	2.87	69.8	1.50	4258	0.25	<DL	314	0.76
			S.D.	10.4	687	3.01	1.35	26.3	0.48	1798	0.16	<DL	61.6	0.32
DNP-1-08 (n = 9)	II	ZK4541	Min.	0.39	428	1.54	0.75	20.0	0.16	2391	<DL	0.58	91.3	0.02
		(214 m)	Max.	24.3	5930	13.7	17.4	141	4.58	5920	<DL	0.63	299	1.11
			Mean	10.1	3336	7.37	6.46	69.1	1.86	3924	<DL	0.61	189	0.60
			S.D.	8.24	2211	3.48	5.29	34.7	1.41	1417	<DL	0.04	77.1	0.39
DNP-1-09 (n = 9)	II	ZK4541	Min.	7.98	1510	35.5	2.62	19.9	2.52	2160	0.14	0.32	255	0.40
		(213 m)	Max.	156	4650	103	20.0	94.3	12.1	10,560	0.38	0.86	559	1.41
			Mean	57.5	2719	65.4	8.65	49.3	5.10	5459	0.22	0.47	399	0.83
			S.D.	58.3	1099	24.9	5.65	26.7	3.06	2527	0.11	0.23	96.5	0.40
DNP-1-10 (n = 8)	II	ZK4541	Min.	4.96	1709	0.24	0.49	9.10	0.01	1631	0.09	0.55	271	0.24
		(212 m)	Max.	163	4800	81.8	16.3	134	5.61	5330	0.72	0.61	406	1.56
			Mean	35.5	3483	27.4	6.30	74.5	1.53	3747	0.41	0.58	349	0.95
			S.D.	57.0	987	28.4	5.48	39.2	1.90	1458	0.45	0.04	42.9	0.55
DNP-2-07 (n = 5)	II	ZK3725	Min.	12.2	2040	0.38	1.53	87.8	0.05	2800	0.12	0.27	158	0.60
		(367 m)	Max.	33.7	7360	6.22	15.0	236	0.63	5529	0.18	0.84	318	3.02
			Mean	19.4	4766	2.07	6.91	130	0.18	3790	0.15	0.54	224	1.43
			S.D.	9.23	2016	2.80	4.93	62.5	0.25	1165	0.04	0.27	74.2	0.92
DNP-3-05 (n = 7)	II	ZK8529	Min.	12.5	4720	1.46	0.08	24.7	0.07	2060	<DL	0.23	343	0.41
		(294 m)	Max.	36.0	8540	23.5	0.75	85.4	0.98	11,400	<DL	0.96	1050	2.17
			Mean	21.7	6249	11.7	0.44	51.4	0.34	6459	<DL	0.60	613	1.51
			S.D.	8.64	1555	7.83	0.29	20.6	0.31	3498	<DL	0.52	247	0.66
(n = 53)	II		Min.	0.39	428	0.24	0.08	9.10	0.01	1520	0.09	0.23	91.3	0.02
			Max.	183	8540	121	20.0	236	12.1	11,400	1.10	0.96	1050	3.02
			Mean	33.8	4166	29.8	5.67	69.3	2.02	4682	0.28	0.55	341	0.91
			S.D.	45.5	2064	34.0	5.13	40.0	2.24	2367	0.26	0.22	165	0.59

2011). The Zn-Pb orebodies were locally crosscut by the post-ore NW-trending reverse faults (F2-group) and ENE-trending normal faults (F3-group) in the Danaopo deposit (Fig. 2; Chen et al., 2018).

Twenty-five Zn-Pb orebodies at Danaopo have been identified as stratoid and lenticular shapes, containing approximately 150 Mt ore with an average of 3.1% Zn + Pb (Fig. 2; Yu et al., 2014; Mao, 2016). These orebodies include mainly sulfide ores with minor oxide ores. The sulfide ores exhibit textures of subhedral to anhedral granular/replaced/poikilitic/cataclastic, and are composed of metallic minerals (incl. sphalerite, galena, and pyrite) and non-metallic minerals (incl. calcite, dolomite, barite, and fluorite) (Fig. 2a-l; Wu et al., 2021). Besides, diagenetic, hydrothermal, and supergene periods were identified during the Danaopo Zn-Pb mineralization. There are three mineralization stages that make up the hydrothermal ore-forming period, i.e., early (I), major (II), and late (III) ore-stage (the details were shown in Wu et al., 2021). The Danaopo sphalerites were primarily formed during the main ore-stage (Sp-II), with a minor contribution from the early ore-stage (Sp-I). The Sp-I occurred as anhedral piebald that was enclosed or locally replaced by early stage calcite (Cal-I) (Fig. 3 a, c, e, f, i, and j). The Sp-II was mainly in thick-veined shape and distributed in the edge of main ore-stage lump calcite (Cal-II) (Fig. 3 b, d, g, h, k, and l).

3. Analytical procedures

3.1. Sample preparation

The representative samples studied in this investigation were gathered from three drill holes (i.e., ZK4541, ZK3725, and ZK8529) in the Danaopo deposit. A total of eleven polished thin sections that include two generations of sphalerite and calcite were chose for LA-ICPMS trace element analyses. Additionally, two representative sphalerite grains from the early and main ore stages were selected for LA-ICPMS element maps. Nineteen ore-stage calcite and four post-ore calcite were manually handpicked from sulfide ores and carbonate wallrocks using micro-drill in order to undertake C-O isotope studies.

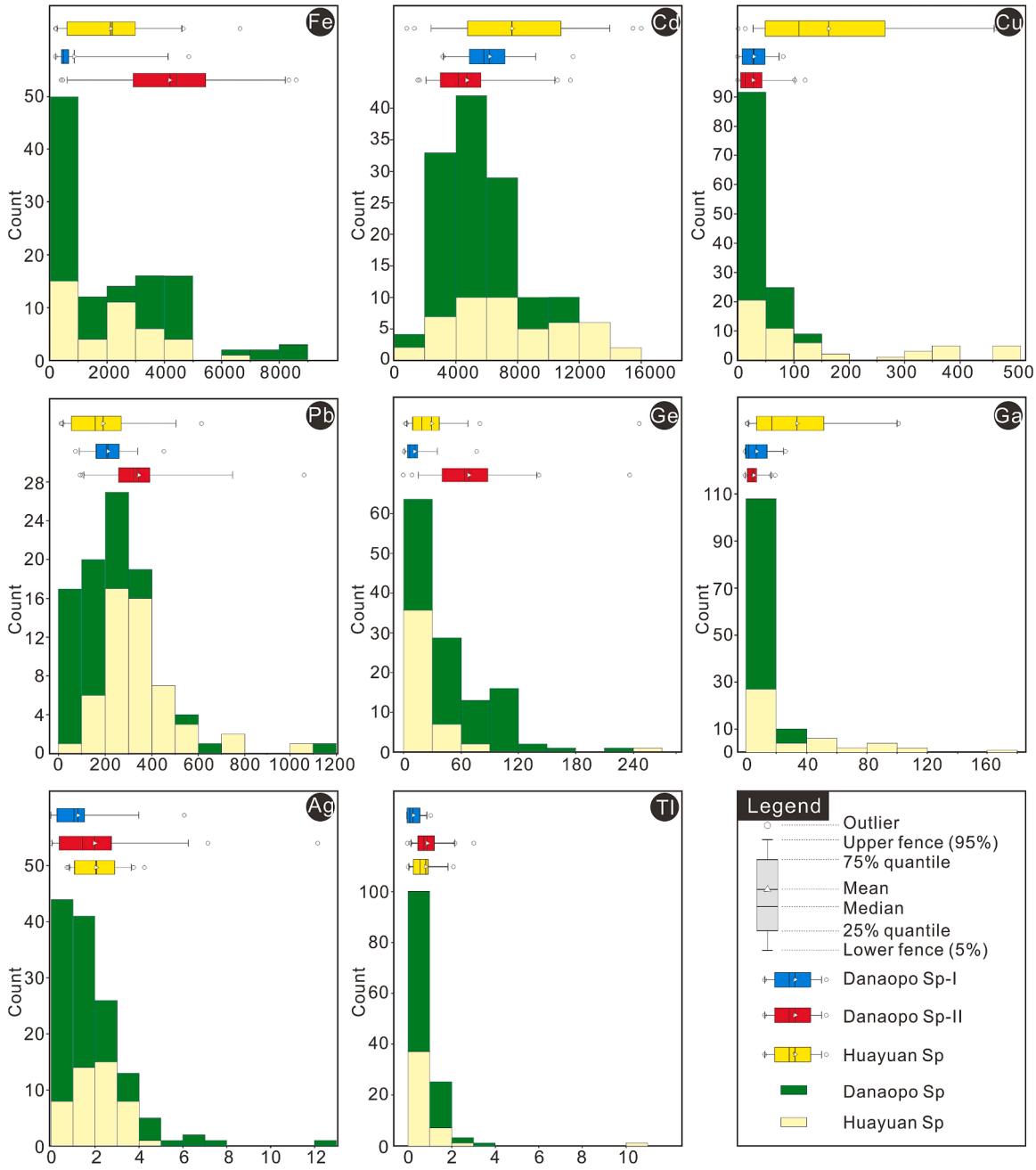

Fig. 4. Histograms showing the comparison of LA-ICPMS trace elements concentration in sphalerite between Danaopo deposit and Huayuan orefield (data of Huayuan sphalerite from Wei et al., 2021c).

3.2. Sphalerite LA-ICPMS multi-element analysis

The in-situ trace element analysis of sphalerite was carried out by LA-ICPMS at the Guangzhou Tuoyan Analytical Technology Co., Ltd., Guangzhou, China, using a NWR Laser ablation system ($\lambda = 193$ nm) coupled to an iCAP RQ ICP-MS instrument and a "wire" signal smoothing device. Helium was used as a carrier gas. A total of 88 spots and 2 elemental maps were selected on sulfide samples covering Sp-I and Sp-II. The analysis was run with a 30 μm spot size and 8 Hz pulse frequency in this study. The following isotopes were quantified: ^{49}Ti, ^{55}Mn, ^{57}Fe, ^{59}Co, ^{60}Ni, ^{65}Cu, ^{66}Zn, ^{71}Ga, ^{72}Ge, ^{75}As, ^{77}Se, ^{107}Ag, ^{111}Cd, ^{115}In, ^{118}Sn, ^{121}Sb, ^{125}Te, ^{204}Pb, and ^{205}Tl. Each analysis took around 50 s to acquire the backdrop information before acquiring the sample data for 40 s. Trace element compositions of sphalerite were calibrated against multiple reference materials (i.e., NIST610, GSE-2G, and GE7) using stoichiometric concentrations of Zn used for sphalerite as an internal standard. The software IOLITE was used to conduct off-line processing of trace element data.

3.3. Bulk C-O isotope analyses

The C-O isotope analyses of the carbonate wallrocks and calcite were performed at State Key Laboratory of Ore Deposit Geochemistry (SKLODG), Institute of Geochemistry, Chinese Academy of Sciences (IGCAS), and measured using a Finnigan MAT-253 gas isotope ratio mass spectrometer. The C-O isotope compositions were assessed using CO_2, which was produced during the reaction of Danaopo calcite with 100% phosphoric acid for 24 h at 72℃. The analytical precision (2σ) for $\delta^{13}C$ values was ± 0.2‰ and for $\delta^{18}O$ values was ± 0.4‰. The carbon isotope composition was reported relative to Vienna Peedee Belemnite

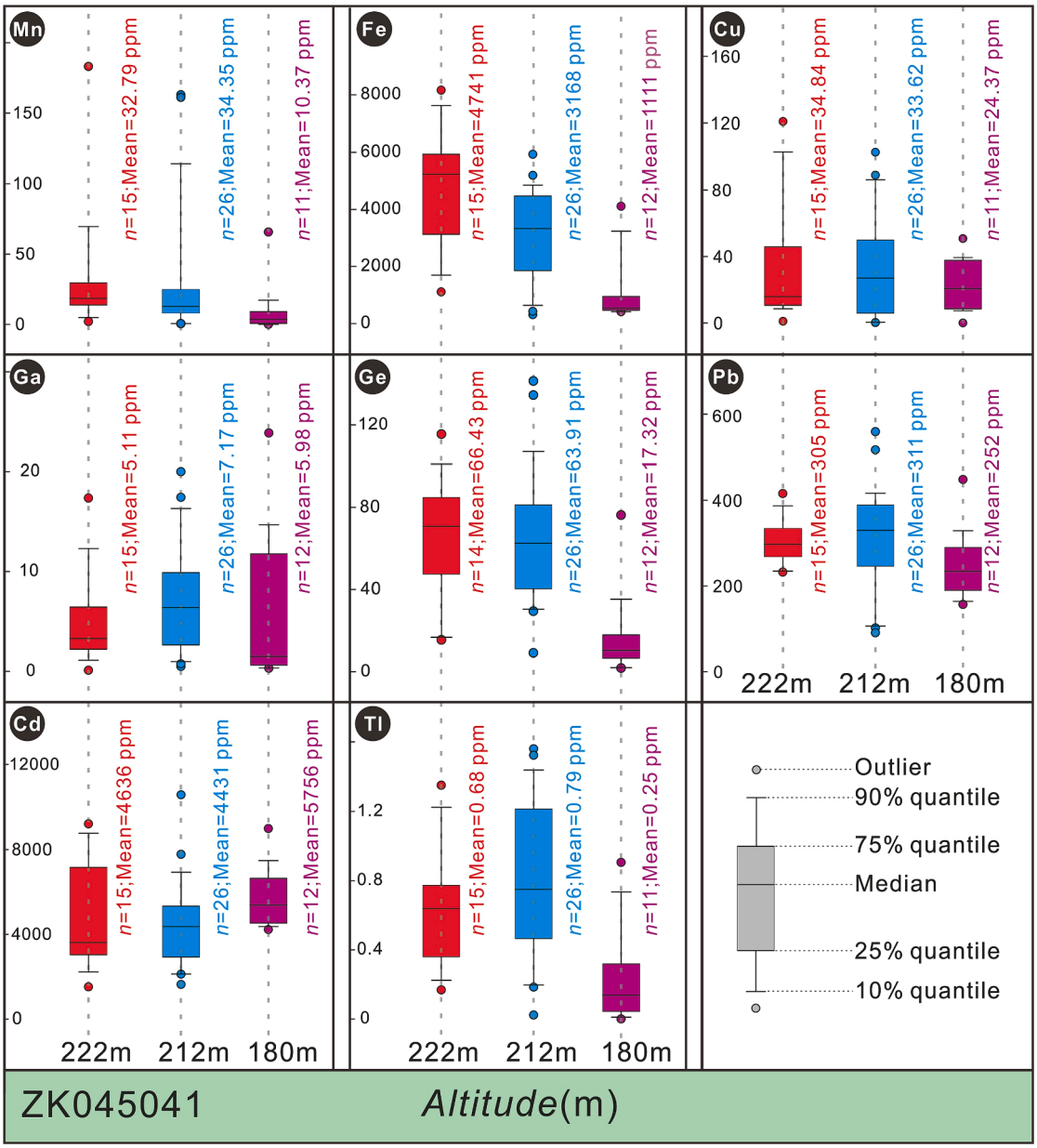

Fig. 5. Boxplot showing trace element contents in sphalerite collected from different altitudes within drill ZK4541 at Danaopo.

(V-PDB), while the oxygen isotope was reported relative to V-PDB and Vienna standard mean ocean water (V-SMOW). The formula $\delta^{18}O_{V\text{-}SMOW} = 1.03086 \times \delta^{18}O_{V\text{-}PDB} + 30.86$ was used to transform the $\delta^{18}O$ values from V-PDB to V-SMOW (Friedman and O'Neil, 1977).

3.4. Calcite LA-ICPMS REE analysis

The calcite REE analysis was conducted by LA-ICPMS at the SKLODG, IGCAS, using a *GeoLas Pro* 193 nm ArF excimer laser coupled to an Agilent 7700x ICP-MS instrument with helium applied as carrier gas during laser ablation. Each analysis included a backdrop capture of 30 s and a sample data acquisition of 50 s. Calcite REE compositions were reported relative to various reference materials (i.e., GOR128-G, ATHO-G, StHs8/80-G, T1-G) combined with an internal standard (Chen et al., 2011). The off-line processing of trace element data was carried out via IOLITE and ICPMSDataCal (Liu et al., 2008; Liu et al., 2010).

4. Results

4.1. Trace elements in sphalerite

The LA-ICPMS trace elements of the Danaopo sphalerite are presented in Table 1 and Fig. 4. The analysis covered 11 samples, including 88 spots and 2 elemental maps, with 35 spots and 1 elemental map for early ore-stage sphalerite (Sp-I) and 53 spots and 1 elemental map for main ore-stage sphalerite (Sp-II). The complete datasets are listed in Supplemental Material 1.

The most prevalent trace element in Danaopo sphalerite is cadmium (Cd), with quantities averaging 5265 ppm and ranging from 1520 to 11570 ppm. Cd concentration in Sp-I (ranging from 3151 to 11570 ppm, avg. 6147 ppm) are higher than those in Sp-II (1520 to 11400 ppm, avg. 4682 ppm). Iron (Fe) and lead (Pb) contents in sphalerite range from 227 to 8540 ppm (avg. 2842 ppm) and 71.2 to 1050 ppm (289 ppm), respectively. The concentrations of Fe (227–4830 ppm, avg. 830 ppm) and Pb (71.2–449 ppm, avg. 210 ppm) in Sp-I are lower than those in Sp-II, which consist of Fe of 428 to 8540 ppm (avg. 4166 ppm) and Pb of

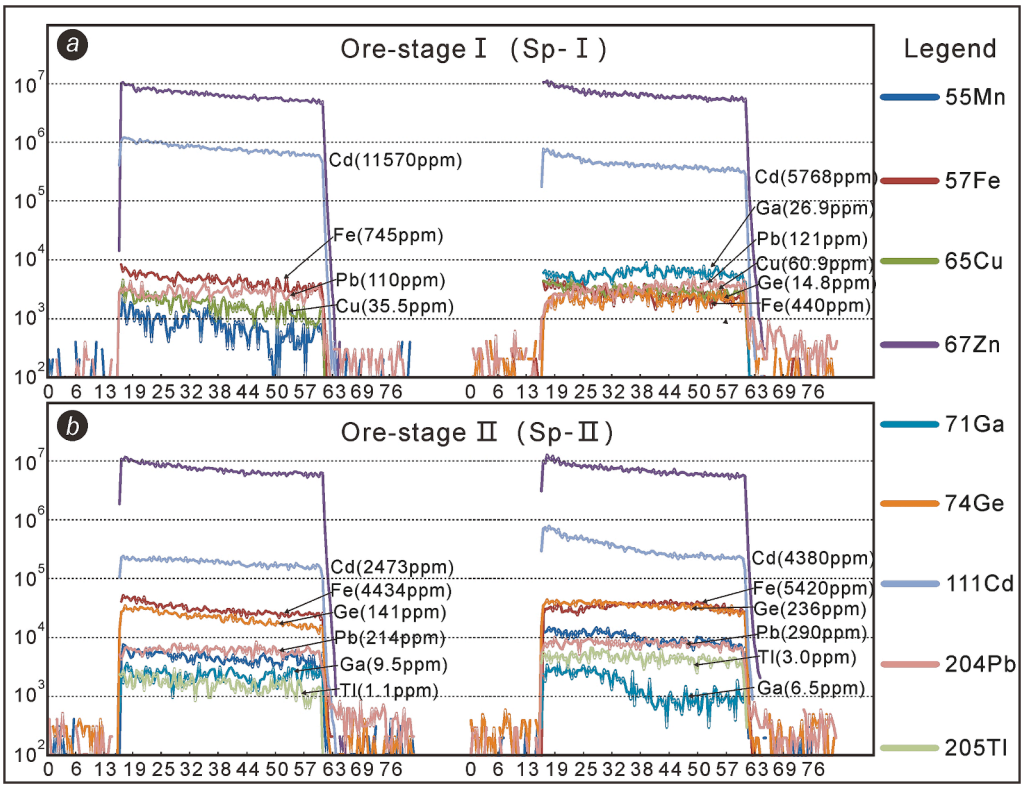

Fig. 6. Representative LA-ICPMS ablation profiles of the Danaopo sphalerite from early and main ore stage.

91.3 to 1050 ppm (avg. 341 ppm).

The critical metals in sphalerite include Germanium (Ge), Gallium (Ga), and Thallium (Tl), with concentrations ranging from 0.73 to 236 ppm (avg. 44.91 ppm), 0.04 to 26.90 ppm (avg. 6.40 ppm), and 0.01 to 3.62 ppm (avg. 0.66 ppm), respectively. In the Sp-II, Ge (9.1 to 236 ppm, avg. 69.3 ppm) and Tl (0.02 to 3.02 ppm, avg. 0.91 ppm) are higher in concentration than in Sp-I (Ge: 0.73–76.2 ppm, avg. 12.1 ppm; Tl: 0.01 to 1.08 ppm, avg. 0.31 ppm), while Ga exhibits slight differences in concentration between Sp-I and Sp-II.

The concentrations of Manganese (Mn), Copper (Cu), Silver (Ag) are from 0.12 to 201 ppm (avg. 30.10 ppm), 0.24 to 121 ppm (avg. 28.68 ppm), and 0.01 to 12.06 ppm (avg. 1.68 ppm), respectively. No significant difference is observed for these elements between Sp-I and Sp-II.

Besides, the Fig. 5 shows that the Cd concentration in sphalerite gradually decreases with increasing elevation in the ZK4541 drill hole. The average Cd contents in the lower orebody (~180 m with avg. Cd of 5756 ppm) are higher than those in the upper orebody (222 m with avg. Cd of 4636 ppm) (Fig. 5). Conversely, Fe, Ge, Pb, and Tl concentrations in sphalerite increase gradually with the increase of elevation (Fig. 5). Sphalerite in the upper orebody has higher average contents of Fe (4741 ppm), Ge (66.00 ppm), Pb (311 ppm), and Tl (0.79 ppm) than the lower orebody that consist Fe of 1111 ppm, Ge of 17.32 ppm, Pb of 252 ppm, and Tl of 0.23 ppm in sphalerite (Fig. 5). Furthermore, the contents of Ti, Co, Ni, As, Se, In, Sn, Sb, and Te in Danaopo sphalerite are mostly below the detection limits.

4.2. C-O isotopes of calcite and country rocks

The carbon and oxygen isotope compositions of the algal limestone and calcite are showed in Table 2 and Figs. 9–10. The Cambrian algal limestone (n = 9) has measured $\delta^{13}C_{PDB}$ and $\delta^{18}O_{SMOW}$ values ranging from −1.88 to + 0.95‰ (avg. −0.85‰) and + 18.76 to + 23.87‰ (avg. + 21.58‰), respectively (Table 2). The $\delta^{13}C_{PDB}$ and $\delta^{18}O_{SMOW}$ values of ore-stage calcite (n = 19) are from −3.93 to −0.12‰ (avg. −1.94‰) and + 14.58 to + 21.19‰ (avg. + 17.93‰), respectively, showing slightly different C-O isotope compositions with horizontal and vertical variation (Table 2, Fig. 10). It is worth noting that four post-ore calcite samples have lower $\delta^{13}C_{PDB}$ values ranging from −8.94 to −7.51‰ (avg. −8.34‰) and heavier $\delta^{18}O_{SMOW}$ values ranging from + 17.37 to + 22.09‰ (mean + 20.78‰) compared to the ore-stage calcite (Table 2). Besides, the theoretical calculated $\delta^{13}C_{CO2}$ and $\delta^{18}O_{fluid}$ values of the ore-stage calcite range from −4.97 to −1.16‰ (avg. −2.98‰) and + 2.44 to + 9.05‰ (avg. + 5.79‰), respectively (Table 2).

4.3. Rare earth elements in calcite

The REE compositions of hydrothermal calcite in the early (Cal-I, *n* = 9) and main (Cal-II, *n* = 11) ore stages at Danaopo are summarized in Table 3 and showed in Fig. 11. The Cal-I has lower total REE contents (ΣREE) of 0.18 to 2.88 ppm with an average of 1.35 ppm, compared to the Cal-II with ΣREE ranging from 1.12 to 51.09 ppm (avg. 10.76 ppm). The REE distribution patterns of all samples normalized to the chondrite values are characterized by LREE enrichment with LREE/HREE ratios of 1.68–17.33 (avg. 7.64) for Cal-I and 3.78–31.29 (avg. 14.35) for Cal-II (Table 3; Fig. 11a, b). The δEu values of Cal-I and Cal-II range from 0.18 to 1.17 (avg. 0.65) and 0.35–0.73 (avg. 0.56), respectively (Table 3; Fig. 11a, b), both showing negative Eu anomalies. Additionally, the $(La/Sm)_N$ of 2.58 to 22.22 (avg. 9.25) and $(Gd/Yb)_N$ of 1.15 to 5.63 (avg. 2.52) for Cal-I are approximately identical to the Cal-II with $(La/Sm)_N$ of 3.29–12.61 (avg. 10.31) and $(Gd/Yb)_N$ of 1.73–5.10 (avg. 3.32), indicating a similar fractionation degree of LREE and HREE for early and main ore stage calcite.

5. Discussion

5.1. Occurrence and incorporation of critical metals in sphalerite

Trace element composition of sphalerite in the Danaopo Zn-Pb deposit is similar to other typical deposits in the Huayuan orefield, such as Limei, Bamaozhai, and Tudiping (Fig. 4;data from Wei et al., 2021c).

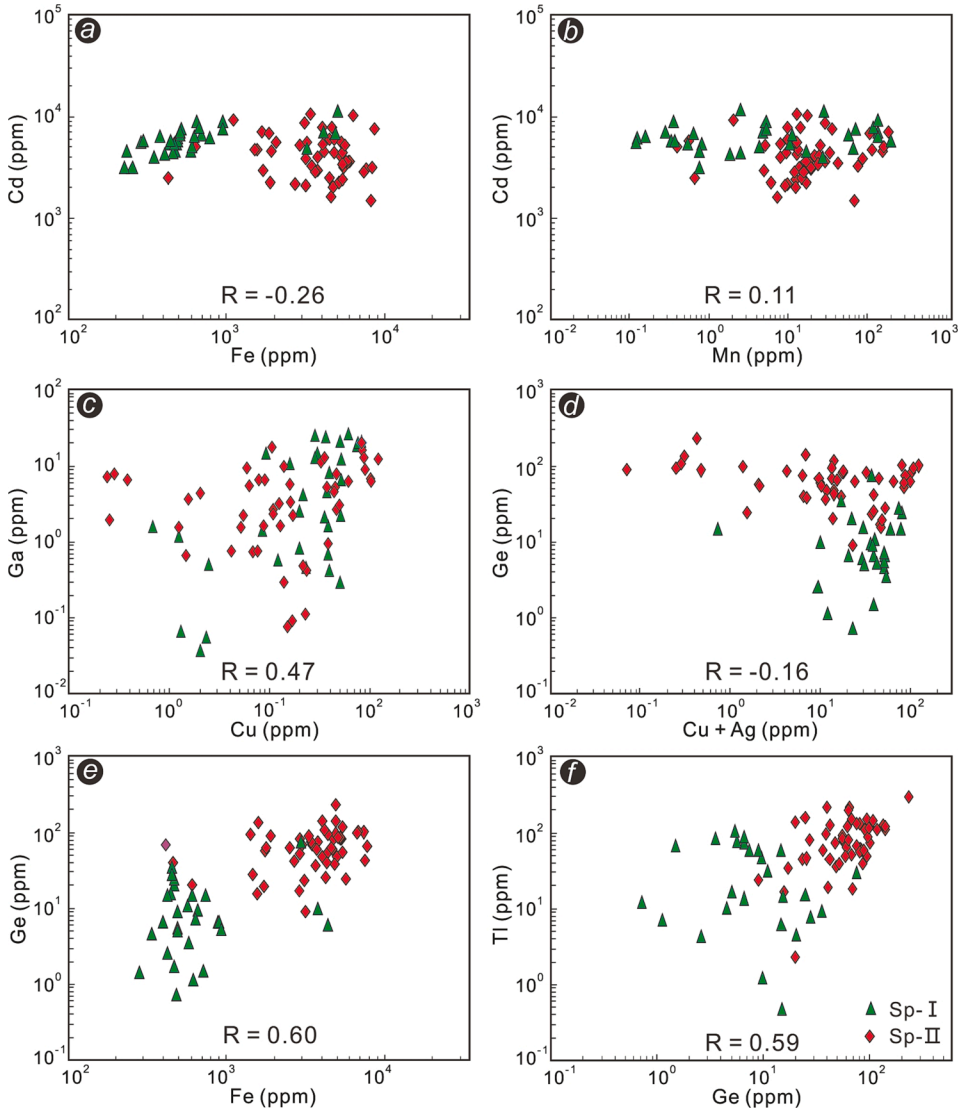

Fig. 7. Correlations plots of (a) Fe vs. Cd, (b) Mn vs. Cd, (c) Cu vs. Ga, (d) Cu + Ag vs. Ge, (e) Fe vs. Ge, and (f) Ge vs. Tl in Danaopo sphalerite.

The Danaopo sphalerite has the distribution of critical metals including Cd (avg. 5265 ppm), Ge (avg. 44.91 ppm), Ga (avg. 6.40 ppm), and Tl (avg. 0.66 ppm), among which Cd and Ge show economic potential. A general survey report suggest that the Danaopo deposit is associated with approximately 65,000 tons of metal Cd that can be comprehensively recycled (Yu et al., 2014). This amount meets the standard of a large scale Cd deposit (>3000 tons). However, Ge was not extracted from Danaopo or any other deposit in the Huayuan orefield. Actually, Ge in sphalerite (avg. 82 ppm; Ye et al., 2011) from the Huize Zn-Pb deposit, China (with 525 tons of Ge metal; Liu et al., 2022) has been effectively recycled with a 79% recovery rate (Ao et al., 2021). Although the average Ge content in Danaopo sphalerite is not remarkable, our data show that Ge is mainly enriched in vein-type sphalerite (Sp-II; Fig. 3 b, d, g-h, k-l) from the upper orebody with an elevation of over 180 m (avg. Ge of 69.3 ppm; Figs. 4–5; Table 1). This indicate that the Danaopo deposit also has the potential for comprehensive Ge utilization.

Unraveling the occurrence mode and enrichment mechanism of critical metals is essential for their comprehensive utilization. LA-ICPMS ablation profiles, elemental maps, and inter-element correlations of the LA-ICPMS can provide significant evidence for the occurrence and incorporation of trace elements in host minerals (Cook et al., 2009; Ye et al., 2011; Belissont et al., 2014; Wei et al., 2019, 2021a). In this study, the LA-ICPMS ablation profiles of Cd, Ga, Ge, and Tl for Sp-I and Sp-II are smooth and flat, similar to those of Zn (Fig. 6 a-b), indicating that these critical metals might show up in sphalerite as solid solutions. Although sub-micrometer particles could not be completely ruled out, the elemental inter-correlations could provide additional restrictions (Li et al., 2020).

Cadmium commonly enters the sphalerite lattice through directly substituting Zn^{2+} (Cook et al., 2009; Ye et al., 2016; Hu et al., 2021). In the Danaopo deposit, Cd and other trace elements show extremely weak correlations in elemental binary plots (Fig. 7a-b) and have poor covariant relationships in LA-ICPMS elemental maps (Fig. 8), indicating that Cd is likely incorporated into the Danaopo sphalerite lattice via direct replacement of Zn^{2+} ($Zn^{2+} \leftrightarrow Cd^{2+}$).

The incorporation mechanism of Ge in sphalerite has always been a subject of debate. Previous studies have proposed various mechanisms, including direct replacement of Zn^{2+} by Ge^{2+} or Ge^{4+}, such as $Zn^{2+} \leftrightarrow Ge^{2+}$ (Cook et al., 2009) and $2Zn^{2+} \leftrightarrow Ge^{4+} + \square$(vacancy) (Cook et al., 2015; Bonnet et al., 2016). Other studies have suggested coupled substitution of Ge^{2+} or Ge^{4+} and mono- and/or bivalent ions of $(Cu \text{ or } Ag)^{+}$ and Cu^{2+} for Zn^{2+}, such as $3Zn^{2+} \leftrightarrow Ge^{4+} + 2(Cu, Ag)^{+}$ (Johan, 1988), $3Zn^{2+} \leftrightarrow Ge^{4+} + 2(Cu, Ag)^{+}$ (Belissont et al., 2014, 2016; Wei et al., 2019; Li et al., 2020; Oyebamiji et al., 2020) and $(n + 1)\ Zn^{2+} \leftrightarrow Ge^{2+} + (n + 1)\ Cu^{2+}$ (Ye et al., 2016). Additionally, coupled substitution of Ge^{4+} and Fe^{2+} for Zn^{2+} has been proposed, such as $4Zn^{2+} \leftrightarrow Ge^{4+} + 2Fe^{2+} +$

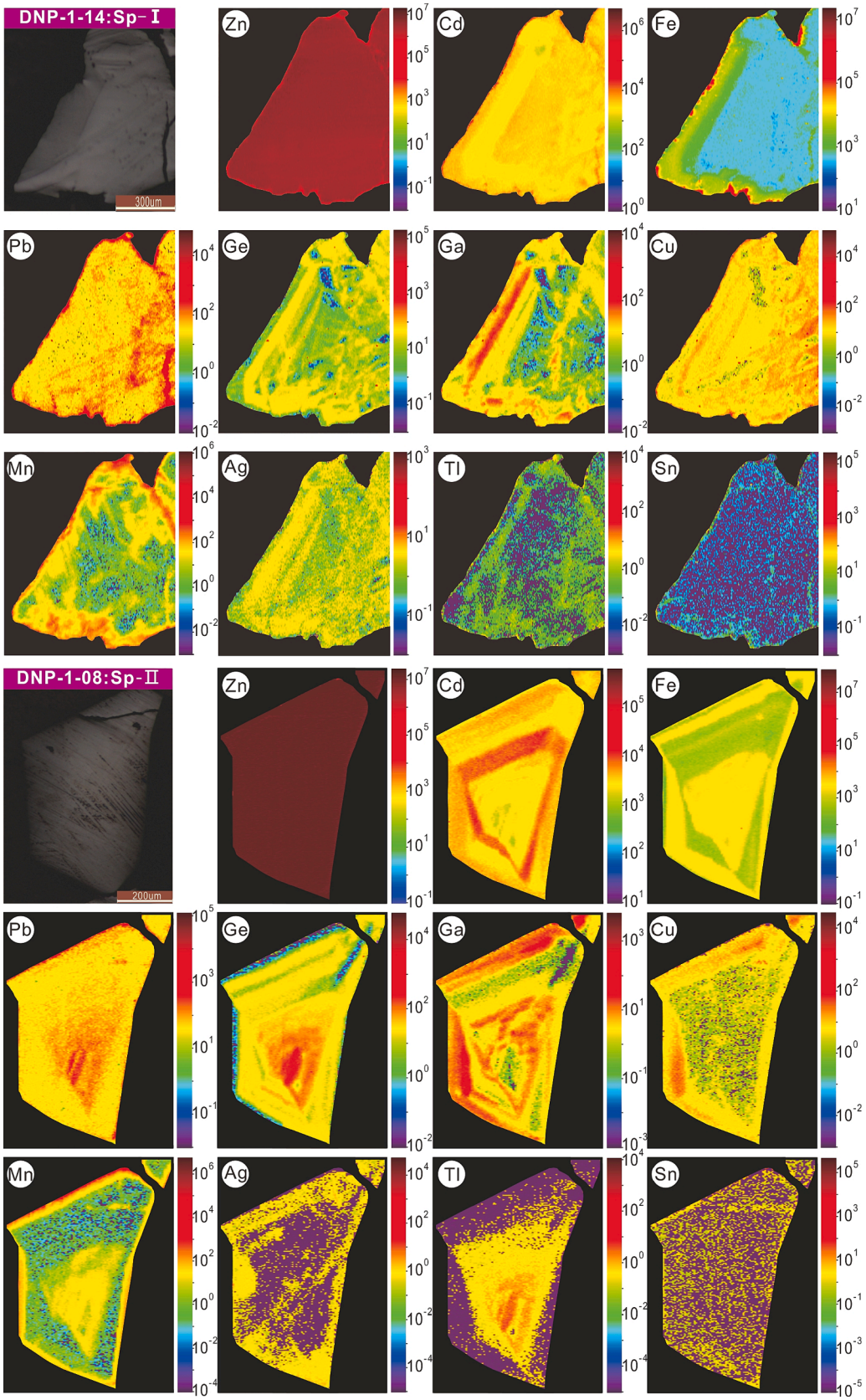

Fig. 8. LA-ICPMS elemental maps of the Danaopo sphalerite in early and main ore stage.

Table 2
$\delta^{13}C$-$\delta^{18}O$ composition of the wallrocks and calcite from the Danaopo deposit.

Sample	Location	Object	$\delta^{13}C_{PDB}$/‰	$\delta^{13}C_{fluid}$/‰	$\delta^{18}O_{SMOW}$/‰	$\delta^{18}O_{fluid}$/‰
DNP-1-01	ZK4541	Algal limestone	−1.58	–	23.03	–
DNP-1-07	ZK4541		−0.31	–	21.24	–
DNP-1-11	ZK4541		−1.88	–	20.33	–
DNP-1-14	ZK4541		−1.29	–	20.83	–
DNP-2-03	ZK3725		0.37	–	18.76	–
DNP-2-06	ZK3725		−1.66	–	21.78	–
DNP-2-07	ZK3725		−0.83	–	21.63	–
DNP-3-04	ZK8529		0.95	–	23.87	–
DNP-3-07	ZK8529		−1.50	–	22.78	–
DNP-1-01	ZK4541	Ore-stage calcite	−2.14	−3.18	20.87	8.73
DNP-1-02	ZK4541		−0.97	−2.01	18.91	6.77
DNP-1-05	ZK4541		−2.46	−3.50	17.54	5.40
DNP-1-07	ZK4541		−0.69	−1.73	16.85	4.71
DNP-1-08	ZK4541		−2.23	−3.27	18.89	6.75
DNP-1-09	ZK4541		−2.19	−3.23	19.17	7.03
DNP-1-10	ZK4541		−1.53	−2.57	21.19	9.05
DNP-1-11	ZK4541		−2.85	−3.89	18.41	6.27
DNP-1-12-1	ZK4541		−1.92	−2.96	18.70	6.56
DNP-1-12-2	ZK4541		−2.62	−3.66	15.94	3.80
DNP-1-13-1	ZK4541		−3.27	−4.31	16.66	4.52
DNP-1-13-2	ZK4541		−2.19	−3.23	20.26	8.12
DNP-1-14	ZK4541		−2.48	−3.52	15.65	3.51
DNP-1-15	ZK4541		−0.12	−1.16	20.54	8.40
DNP-2-01	ZK3725		−1.41	−2.45	15.16	3.02
DNP-2-02	ZK3725		−2.65	−3.69	14.58	2.44
DNP-2-07	ZK3725		−0.50	−1.54	17.21	5.07
DNP-3-02	ZK8529		−0.70	−1.74	18.31	6.17
DNP-3-09	ZK8529		−3.93	−4.97	15.78	3.64
DNP-1-03	ZK4541	Post-ore calcite	−8.85	–	21.82	–
DNP-1-04	ZK4541		−7.51	–	21.85	–
DNP-1-10	ZK4541		−8.07	–	17.37	–
DNP-2-04	ZK3725		−8.94	–	22.09	–

Note: The $\delta^{13}C_{fluid}$ and $\delta^{18}O_{fluid}$ values were calculated via $1000\ln\alpha = -2.4612 + 7.663 \times 10^3/T - 2.988 \times 10^6/T^2$ (Bottinga, 1968) and $1000\ln\alpha = 2.78 \times 10^6/T^2 - 3.39$ (O'Neil et al., 1969), respectively. T = t + 273.15, t is a homogenization temperature (150°C) of fluid inclusions in sphalerite and calcite in the Huayuan orefield.

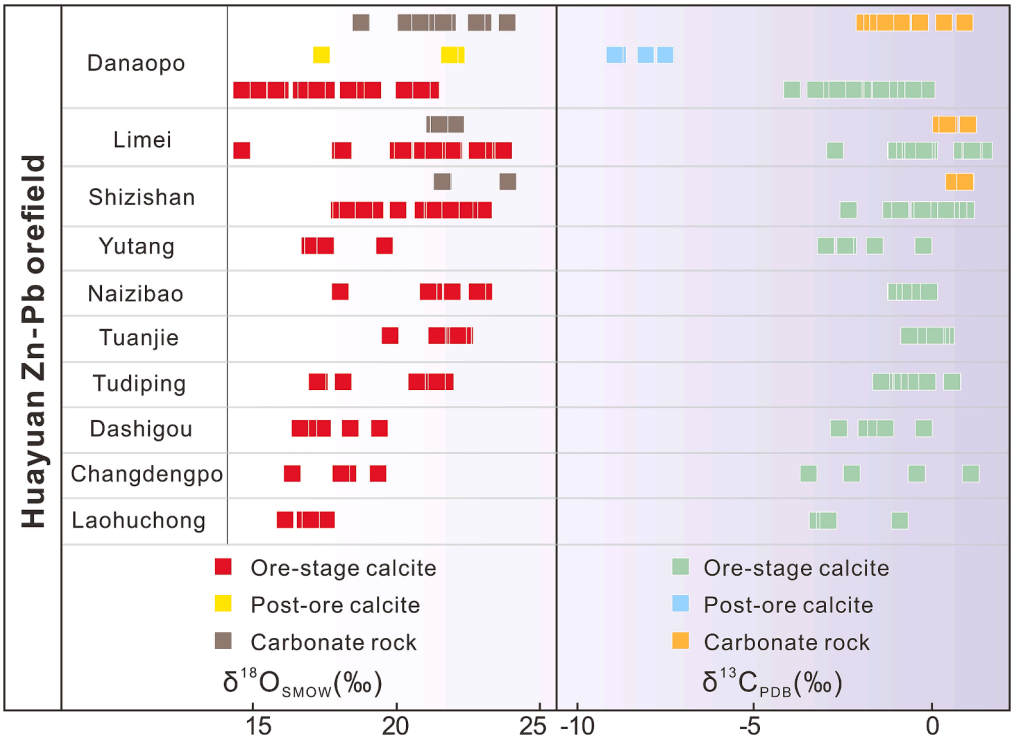

Fig. 9. $\delta^{13}C_{PDB}$-$\delta^{18}O_{SMOW}$ composition of the wallrocks and calcite in the Huayuan Zn-Pb orefield. Data sources: Limei (Xia and Shu, 1995; Cai et al., 2014; Zhou et al., 2017), Shizishan (Cai et al., 2014; Duan, et al., 2014), Yutang (Li et al., 2014), Naizibao (Yang and Lao, 2007), Tuanjie and Dashigou (Zhou et al., 2017), Tudiping (Zhou et al., 2017; Wei, 2017), Changdengpo and Laohuchong (Wei, 2017).

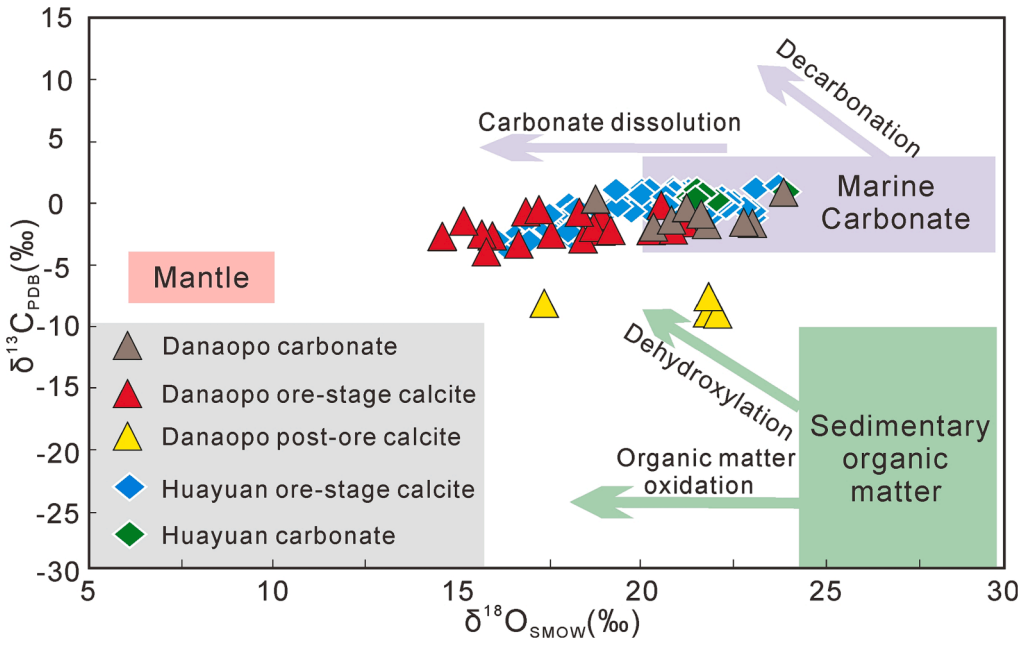

Fig. 10. $\delta^{13}C_{PDB}$-$\delta^{18}O_{SMOW}$ diagram of calcite and carbonate wallrock in the Danaopo deposit (modified after Wei, 2017).

□ (Yuan et al., 2018; Luo et al., 2022). At Danaopo, a weak negative linear correlation (r = -0.16) was observed between Ge and (Cu + Ag) (Fig. 7d). The LA-ICPMS elemental map between Ge and Cu or Ag displayed a poor covariant relationship in Sp-I and Sp-II (Fig. 8), indicating that the substitution of Ge in Danaopo sphalerite could not occur through $3Zn^{2+} \leftrightarrow Ge^{4+} + 2(Cu, Ag)^{+}$ and $(n + 1)\ Zn^{2+} \leftrightarrow Ge^{2+} + (n + 1)\ Cu^{2+}$. In contrast, good positive correlations were identified between Ge and Fe (r = 0.60; Fig. 7e) and Ge and Tl (r = 0.59; Fig. 7f). The covariant relationships among Fe, Ge and Tl were evident, especially in Ge-rich Sp-II (Fig. 8), which indicate that the substitution of Ge in sphalerite has a tight connection to Fe and Tl. Germanium is typically found as Ge^{4+} in nature (Wood and Samson, 2006; Höll et al., 2007). Previous research claimed that Ge and Fe were respectively present in Ge-rich sphalerite as Ge^{4+} and Fe^{2+} using X-ray Absorption Near Edge Structure (XANES) (Cook et al., 2015; Belissont et al., 2016). Thus, Ge is most likely incorporated into the Danaopo sphalerite lattice through $4Zn^{2+} \leftrightarrow Ge^{4+} + 2Fe^{2+} + □$. Besides, based on thermodynamic evidence, Tl^{+} was predominant in hydrothermal solutions (Xiong, 2007; Zhuang et al., 2019). Minor Ge may enter the sphalerite lattice via $3Zn^{2+} \leftrightarrow Ge^{4+} + 2Tl^{+}$ in view of the clear correlation between Ge and Tl (Fig. 7f). But our investigation cannot exclude the substitution of $2Zn^{2+} \leftrightarrow Ge^{4+} + □$.

Gallium is generally present in the sphalerite lattice as a trivalent ion (Cook et al., 2009). Three substitution mechanisms between Ga^{3+} and Zn^{2+} reported in recent years are as follows, (1) direct substitution of Ga^{3+} for Zn^{2+} ($3Zn^{2+} \leftrightarrow 2\ Ga^{3+} + □$(vacancy); Bonnet et al., 2016), (2) coupled substitution of Ga^{3+} and monovalent ions $(Cu, Ag)^{+}$ for Zn^{2+} ($2Zn^{2+} \leftrightarrow Ga^{3+} + (Cu, Ag)^{+}$; Cook et al., 2009; Bonnet et al., 2016), and (3) coupled substitution of Ga^{3+}, Sn^{4+}, and Cu^{+} for Zn^{2+} ($4Zn^{2+} \leftrightarrow Ga^{3+} + Sn^{4+} + Cu^{+} + □$; Zhuang et al., 2019). At Danaopo, Ga and Cu exhibit a positive linear correlation (r = 0.47; Fig. 7c). However, the distribution of Ga in Sp-I and Sp-II displays zonal features that are inhomogeneous and clearly distinct from those of Cu (Fig. 8). Therefore, the coupled replacement of $4Zn^{2+} \leftrightarrow Ga^{3+} + Sn^{4+} + Cu^{+} + □$ and $2Zn^{2+} \leftrightarrow Ga^{3+} + Cu^{+}$ could be excluded. Instead, Ga is probably dominated by the substitution of $3Zn^{2+} \leftrightarrow 2\ Ga^{3+} + □$ into the Danaopo sphalerite lattice.

5.2. Nature of ore-forming fluid

5.2.1. Sources of C and O

The carbon and oxygen isotopes are a valuable tool for determining the origin of ore-forming fluids and providing indicators for mineral precipitation mechanisms and physicochemical conditions in carbonate-host hydrothermal Pb-Zn deposits (Zheng and Wang, 1991; Li et al., 2015). There are three potential sources of C and O in hydrothermal mineralization fluids, including mantle magma ($\delta^{13}C_{PDB}$ = -8‰ to −4‰, $\delta^{18}O_{SMOW}$ = +6‰ to + 10‰; Taylor et al., 1967), organic matters in sediments ($\delta^{13}C_{PDB}$ = -30‰ to −10‰, $\delta^{18}O_{SMOW}$ = +24‰ to + 30‰; Kump and Arthur, 1999), and marine carbonate rocks ($\delta^{13}C_{PDB}$ = -4‰ to + 4‰, $\delta^{18}O_{SMOW}$ = +20‰ to + 30‰; Veizer and Hoefs, 1976). At Danaopo, the measured $\delta^{13}C_{PDB}$ (-3.93 to −0.12‰; mean −1.94‰) and $\delta^{18}O_{SMOW}$ (+14.58 to + 21.19‰; mean + 17.93‰) compositions of ore-stage calcite resemble those of the typical Pb-Zn deposits in Huayuan orefield (e.g., Limei, Shizishan, Tudiping etc.). These deposits have calcite $\delta^{13}C_{PDB}$ of −3.46 to + 1.50‰ (mean −0.50‰) and $\delta^{18}O_{SMOW}$ of + 14.59 to + 23.74‰ (mean 20.16‰) (Fig. 9; Xia and Shu, 1995; Li et al., 2014; Cai et al., 2014; Zhou et al., 2017; Wei, 2017 and reference therein), indicating that each Zn-Pb deposit in Huayuan orefield could have identical carbon and oxygen source.

The measured $\delta^{13}C_{PDB}$ values of −3.93 to −0.12‰ (mean −1.94‰) and calculated $\delta^{13}C_{fluid}$ values of −4.97 to −1.16‰ (mean −2.98‰) for the ore-stage calcite (Table 2) overlap with those of marine carbonate rocks ($\delta^{13}C_{PDB}$ = -4‰ ~ +4‰, Veizer and Hoefs, 1976), indicating that the ore-host algal limestone may be the source of carbon in Danaopo hydrothermal calcite. Moreover, the $\delta^{13}C_{PDB}$ values of post-ore calcites (-8.94 to −7.51‰, mean −8.34‰) are lower than those of marine carbonate rocks and approximately close to organic matter ($\delta^{13}C_{PDB}$ = -30 to −10‰; Kump and Arthur, 1999). These post-ore calcites plot close to the sedimentary organic matter dehydroxylation (Fig. 10), indicating an additional $\delta^{13}C$-depleted contribution from organic matter to calcite after Zn-Pb mineralization, in agreement with the Zhugongtang deposit, China (Wei et al., 2021b). In the $\delta^{13}C_{PDB}$ vs. $\delta^{18}O_{SMOW}$ plot, most of the ore-stage calcite from typical Zn-Pb deposits, including Danaopo, Limei, and Shizishan in the Huayuan orefield, plot as a horizontal linear trend near the marine carbonate dissolution baseline (Fig. 10). This suggests that there was an interaction between hydrothermal fluid and wallrocks during the ore formation (Zheng and Hoefs, 1993). Thus, it can be concluded that the carbon in Danaopo ore-forming fluid was mainly originated the dissolution of Qingxudong Fm algal limestone of the lower Cambrian.

It is commonly accepted that the oxygen isotope of the ore-forming

Table 3
REE composition of calcite from the Danaopo deposit ($\times 10^{-6}$).

Sample	Mineral	La	Ce	Pr	Nd	Sm	Eu	Gd	Tb	Dy	Ho	Er	Tm	Yb	Lu	Y	ΣREE	LREE	HREE	L/H	δEu
DNP-1-03	Calcite-I	0.83	1.00	0.10	0.39	0.04	0.01	0.04	<DL	0.04	0.01	0.02	<DL	0.02	<DL	0.23	2.51	2.37	0.14	17.33	1.10
DNP-1-03		1.03	1.15	0.10	0.36	0.05	0.01	0.04	0.01	0.05	0.01	0.05	0.01	0.02	<DL	0.40	2.88	2.70	0.19	14.47	0.52
DNP-1-03		0.28	0.35	0.04	0.12	0.06	0.01	0.04	0.01	0.05	0.01	0.02	<DL	0.01	<DL	0.36	1.01	0.86	0.15	5.76	0.78
DNP-1-03		0.11	0.14	0.02	0.06	0.01	<DL	0.02	<DL	0.01	<DL	0.01	<DL	<DL	<DL	0.09	0.40	0.35	0.06	6.32	0.18
DNP-1-14		0.03	0.03	0.01	0.03	0.01	<DL	0.02	<DL	0.01	<DL	0.02	<DL	0.01	<DL	0.19	0.18	0.11	0.07	1.68	0.42
DNP-1-14		0.51	0.73	0.10	0.42	0.03	0.02	0.05	0.01	0.06	0.01	0.02	<DL	0.02	<DL	0.42	2.00	1.81	0.18	9.90	1.17
DNP-1-14		0.33	0.52	0.07	0.37	0.09	0.01	0.07	0.01	0.07	0.01	0.04	0.01	0.04	<DL	0.64	1.65	1.39	0.25	5.48	0.44
DNP-1-14		0.15	0.20	0.03	0.19	0.05	0.01	0.04	0.01	0.03	0.01	0.03	<DL	0.02	<DL	0.27	0.79	0.64	0.15	4.39	0.58
DNP-1-14		0.12	0.18	0.03	0.18	0.04	0.01	0.04	<DL	0.05	0.01	0.02	0.01	0.02	<DL	0.31	0.71	0.55	0.16	3.42	0.69
DNP-1-07	Calcite-II	8.00	20.78	2.85	10.94	2.42	0.38	2.01	0.27	1.52	0.31	0.77	0.11	0.63	0.09	9.61	51.09	45.37	5.71	7.94	0.52
DNP-1-07		0.56	0.96	0.14	0.59	0.15	0.04	0.17	0.02	0.17	0.03	0.12	0.02	0.09	0.01	1.39	3.08	2.45	0.64	3.83	0.73
DNP-1-07		2.40	2.57	0.36	1.59	0.23	0.05	0.22	0.03	0.17	0.03	0.08	0.01	0.07	0.01	1.19	7.79	7.19	0.60	11.89	0.61
DNP-1-07		0.22	0.32	0.05	0.22	0.07	0.01	0.06	0.01	0.07	0.02	0.05	0.01	0.02	<DL	0.45	1.12	0.89	0.23	3.78	0.60
DNP-1-10		4.02	5.20	0.51	1.99	0.24	0.04	0.15	0.02	0.10	0.02	0.06	0.01	0.03	<DL	0.52	12.40	12.02	0.38	31.29	0.67
DNP-1-10		2.25	2.86	0.28	1.04	0.17	0.02	0.11	0.01	0.09	0.02	0.05	0.01	0.04	<DL	0.58	6.96	6.62	0.34	19.65	0.40
DNP-1-10		4.17	5.33	0.54	2.00	0.30	0.04	0.23	0.02	0.15	0.02	0.07	0.01	0.04	0.01	0.80	12.93	12.38	0.55	22.48	0.53
DNP-1-10		0.72	0.97	0.12	0.39	0.06	0.01	0.05	0.01	0.05	0.01	0.04	<DL	0.02	<DL	0.44	2.46	2.27	0.19	12.02	0.60
DNP-1-10		2.33	2.95	0.31	1.32	0.17	0.03	0.15	0.02	0.10	0.02	0.07	0.01	0.04	0.01	0.76	7.54	7.11	0.43	16.43	0.58
DNP-1-10		2.03	2.75	0.32	1.14	0.18	0.02	0.12	0.02	0.13	0.02	0.07	0.01	0.07	0.01	1.00	6.88	6.43	0.45	14.16	0.35
DNP-1-10		1.87	2.41	0.27	0.95	0.15	0.03	0.13	0.02	0.11	0.02	0.06	0.01	0.04	0.01	0.84	6.06	5.67	0.39	14.41	0.57

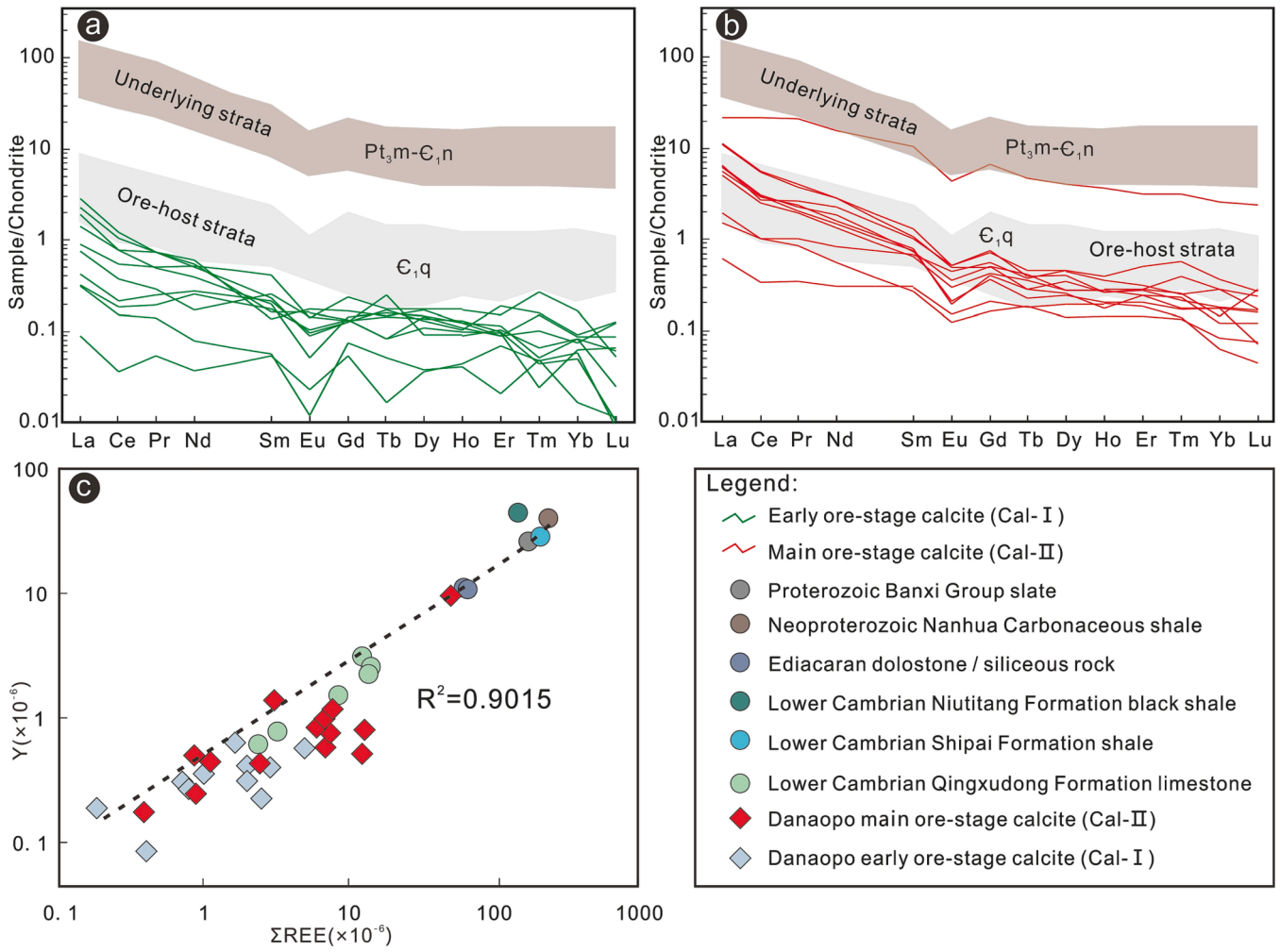

Fig. 11. (a, b) Comparison diagram of REE compositions of calcite in early and main ore stage, ore-host and underlying strata in the Danaopo deposit; (c) Y-ΣREE correlation diagram of the Danaopo ore-stage calcite and potential source rocks (the REE data of the potential source rocks was sourced from Wei et al., 2017).

fluid ($\delta^{18}O_{fluid}$) can approximately represent that of the H_2O in fluid inclusion ($\delta^{18}O_{H2O}$) when isotope exchange reaches equilibrium (Zheng, 1999; Zhou et al., 2018b). The experimental analysis of $\delta^{18}O_{SMOW}$ values (+14.58 to + 21.19‰, avg. + 17.93‰; Table 3; Fig. 10) of the Danaopo ore-stage calcites are lower than those of the ore-host carbonate rocks (+18.76 to + 23.87‰, avg. + 21.58‰; Table 3; Fig. 10). This implies that the Cambrian algal limestone was not the only oxygen source. Besides, the calculated $\delta^{18}O_{fluid}$ values of ore-stage calcite from Danaopo (+5.23 to + 9.95‰, avg. + 8.64‰; Table 2) and Huayuan orefield (+2.45 to + 11.60‰, avg. + 8.02‰; Li et al., 2014; Zhou et al., 2017; Wei, 2017 and references therein) are far lower than the oxygen isotope composition of marine carbonate rocks ($\delta^{18}O_{SMOW}$ = +20‰ ~ +30‰; Veizer and Hoefs, 1976), which indicate a mixing oxygen source from ore-host algal limestone and $\delta^{18}O$-depleted hydrothermal fluid (Ohmoto, 1986). This $\delta^{18}O$-depleted fluid may be categorized as basinal brine ($\delta^{18}O$ = +4‰ ~ +10‰; Talor et al., 1967), given the low temperature, medium–high salinity of the ore-forming fluid and tectonic setting of the foreland basin for the Huayuan orefield (Liu and Zheng, 2000; Duan et al., 2014; Wei, 2017). Hence, the oxygen in the Danaopo hydrothermal calcite could be sourced from a binary mixing of the ore-host algal limestone and basinal hot brine.

5.2.2. *Source of REEs*

Rare earth elements commonly migrate as complexes in the hydrothermal fluid and enter Ca-rich minerals such as calcite, dolomite via the substitution of Ca^{2+} ions (Huang et al., 2010; Luo et al., 2019). This suggests that the REEs composition of hydrothermal calcite may reflect the nature of REE in the mineralization fluid (Huston et al., 1995; Souissi et al., 2013). At Danaopo, the REE distribution patterns of calcite in the early ore-stage (Cal-I; Fig. 11a) are similar to those in the main ore-stage (Cal-II; Fig. 11b). However, the REEs concentration of Cal-I (avg. 1.35 ppm) is obviously lower than that of Cal-II (avg. 10.76 ppm) (Table 3), which possibly imply a different REE source for Cal-I and Cal-II. The correlation between Y and ΣREE of hydrothermal minerals can be utilized to determine the origin of REEs in the ore deposit (Bau and Möller, 1995; Cherniak et al., 2001; Schönenberger et al., 2008). Fig. 11c demonstrate a significant positive association (r^2 = 0.90) among ore-stage calcites, ore-host and footwall sedimentary sequences, and basement metamorphic rocks, indicating a close genetic relationship between Danaopo hydrothermal calcite and these regional sedimentary and basement rocks.

The REE distribution pattern of Cal-I falls within the field of ore-host algal limestone and is distal to the rocks from Proterozoic Banxi Gp to Cambrian Niutitang Fm (Fig. 11a), indicating that the REEs in Cal-I was mainly sourced from the wallrocks. In contrast, the Cal-II is distributed between the above-mentioned potential REE source rocks (Fig. 11a), which is indicative of a mixed REE origin in the main ore-forming stage. The ore-host algal limestone with REEs of 2.39–14.30 ppm (Wei et al., 2017) cannot provide enough REE for Cal-II with REEs of 1.12–51.09 ppm, as confirmed by the extremely low REE content in leachate from carbonate rocks in fluid simulation experiments (Michard, 1989; Ohr et al., 1994). A REE-rich end-member could be incorporated into the Cal-

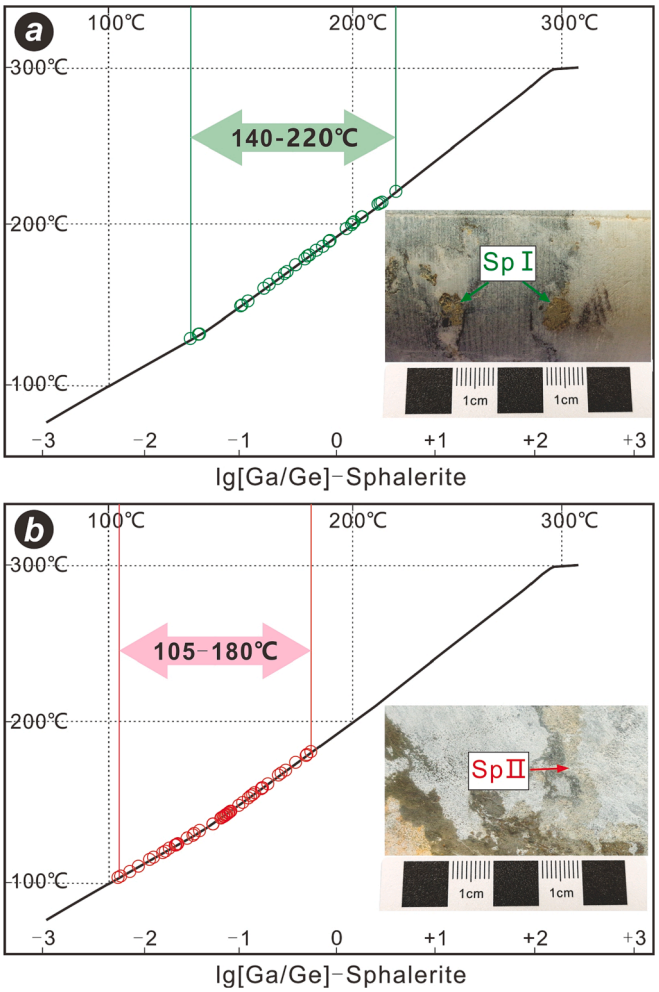

Fig. 12. Lg (Ga/Ge) - T diagram of Danaopo sphalerite from early and main ore stage (modified after Wei et al., 2021c).

II at Danaopo, such as metamorphic basement rocks (avg. ΣREE = 169 ppm) of the Proterozoic Banxi Gp and sedimentary sequence (ΣREE = 62.6–212 ppm) of the Ediacaran Doushantuo Fm to Cambrian Shipai Fm (Wei et al., 2017), as supported by their positive Y-ΣREE correlation (Fig. 11c). Hence, we conclude that the REE in Cal-I was mainly derived from the ore-host Cambrian algal limestone, while the REE in Cal-II was sourced from the ore-bearing carbonate sequence with a significant contribution from the underlying sedimentary and Proterozoic metamorphic basement rocks.

5.2.3. Physical-chemical conditions (Eh and T)

The Eu anomaly (δEu) of REEs is an useful indicator of the redox conditions during mineral precipitation, as it is sensitive to the temperature (*T*) and oxygen fugacity (f_{O2}) of the ore-forming fluid (Sverjensky, 1984; Bau, 1991). Eu predominantly migrates with the hydrothermal fluid as Eu^{3+} in a low-*T* (<100 ℃) and high f_{O2} environment, resulting in a positive Eu anomaly (δEu > 1). In contrast, the ore-forming fluid mostly carries Eu^{2+} in a medium-*T* (100 ℃ < T < 200 ℃) and reductive environment, which results in a negative Eu anomaly (δEu < 1) (Sverjensky, 1984). At Danaopo, both Cal-I and Cal-II exhibit negative Eu anomalies (Fig. 11a, b), with average δEu values of 0.65 and 0.56, respectively (Table 3). This suggests that the mineralization fluid was reductive during both the early and main ore stages. Furthermore, there is a decreasing trend in δEu from Cal-I to Cal-II, indicating that the ore-forming fluid was more reducible during the main ore stage, which was more conducive to the precipitation of ore metals. This observation explains the different sphalerite texture between early (low-grade piebald sphalerite; Fig. 3a, c) and main (high-grade veined sphalerite; Fig. 3b, d) ore stage.

The temperature of the ore-forming fluid has a significant impact on the composition of trace elements in sphalerite (Möller, 1987; Cook et al., 2009; Zou et al., 2012; Frenzel et al., 2016). According to Möller (1987), the lg(Ga/Ge) value of sphalerite is an effective indicator for the temperature of metal-bearing initial fluids. In recent years, the mineralization temperature of the Zn-Pb deposit has frequently been constrained using the sphalerite Ga-Ge thermometer (Hu et al., 2014; Wei et al., 2021c). In the Danaopo deposit, the calculated lg(Ga/Ge) of Sp-I and Sp-II are plotted in the crystallization temperature field of 140–220℃ (Fig. 12a) and 105–180℃ (Fig. 12b), respectively. This indicates a low-temperature mineralization environment during sphalerite precipitation, as supported by the homogenization temperature of 100–200℃ in sphalerite fluid inclusions in the Huayuan orefield (Liu and Zheng, 2000; Cai et al., 2014; Zhou et al., 2014).

5.3. Ore genesis

The trace element endowments in sphalerite are considered a reliable fingerprint for classifying various genetic kinds of Zn-Pb deposits (Cook et al., 2009; Ye et al., 2011; Belissont et al., 2014; Hu et al., 2021; Wei et al., 2021a). The LA-ICPMS trace elements composition in sphalerite from MVT, VMS, and skarn-type Zn-Pb deposits in China were summarized: MVT deposits are relatively enriched in Cd, Ga, Ge, and insignificant in Fe, Mn, In, Sn; VMS deposits are characterized by enrichment of Fe, Mn, In, and deficiency of Cd, Ga, Ge; Skarn-type deposits are generally rich in Mn, Co, and poor in Fe, In, Sn (Ye et al., 2011). Hence, some binary plots of sphalerite trace elements can differentiate Zn-Pb deposits of different genetic types (Ye et al., 2011, 2016; Li et al., 2020; Hu et al., 2021). At Danaopo, most sphalerite samples fall into the field of the MVT deposit but are distal to the VMS and skarn-type deposit (Fig. 13a-f), indicating that the Danaopo could belong to MVT Zn-Pb deposit, which is also supported by the Danaopo pyrite trace elements evidence (Wu et al., 2020).

Radiogenic isotope geochronological evidence suggests that Zn-Pb mineralization in the Huayuan orefield occurred between the Middle Ordovician and Early Devonian periods (ca. 490–410 Ma; Duan et al., 2014; Tan et al., 2018; Zhou et al., 2021). This mineralization event was contemporaneous with the hydrothermal ore-forming event induced by the Caledonian collision orogeny (Yao and Li, 2016; Hu et al., 2022). The Danaopo deposit, irrelevant with regional magmatism, is a typical carbonate hosted epigenetic Zn-Pb deposit in the WHEGMB (Mao, 2016; Wu et al., 2021). The geology-geochemistry features of the Danaopo deposit are summarized as follows: (i) tectonic background (carbonate platform margin slope facies; Yang and Lao, 2007); (ii) ore-host rocks (Lower Cambrian Qingxudong Fm algal limestone; Fig. 2); (iii) ore-controlling structure (F_1-group generated by Huayuan-Zhangjiajie fault movement; Fig. 2); (iv) orebody occurrences (stratoid and lenticular; Figs. 2–3); (v) mineral compositions (sphalerite, pyrite, galena, calcite, and barite; Fig. 3a-l); (vi) ore textures (open-space filling and hydrothermal metasomatism, i.e., sphalerite occurred as veined or disseminated infill in algal limestone and calcite present in nodular and zebra (stripes) textures; Fig. 3a-d); (vii) ore-forming fluid (low-temperature and low f_{O2} reductive basinal brine as supported by sphalerite Ga-Ge thermometer and calcite C-O isotopes and REE features; Figs. 10–12); (viii) precipitation mechanism (mixing of local reduced sulfur and multi-source ore metals; Wu et al., 2021). These features are similar to those of representative Zn-Pb deposits in the WHEGMB (e.g., Niujiaotang, Limei, Shizishan, and Yutang; Cai et al., 2014; Zhou et al., 2017; Wei et al., 2021c; Hu et al., 2022; Zhou et al., 2022), as well as typical MVT Zn-Pb deposits worldwide (Bradley and Leach, 2003; Leach et al., 2010). Overall, the Danaopo deposit is best categorized as an MVT Zn-Pb deposit.

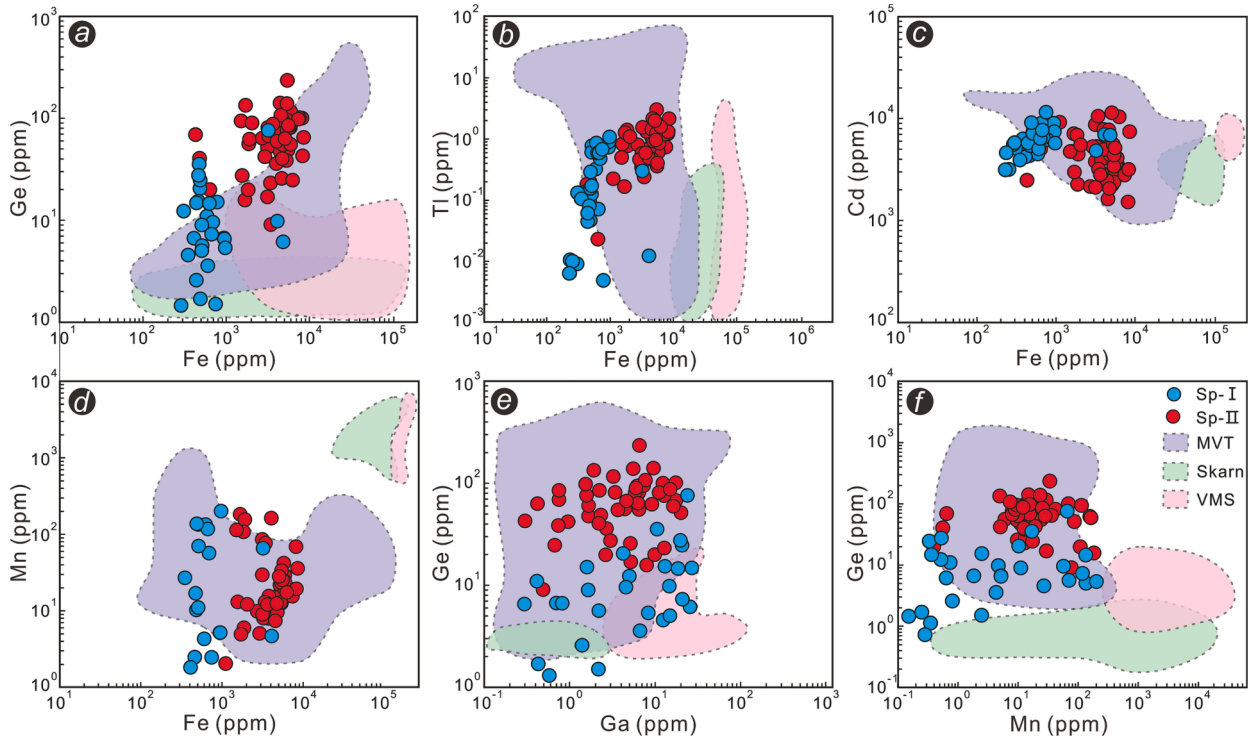

Fig. 13. Comparison of sphalerite trace element compositions between the Danaopo deposit and typical genetic-type Zn-Pb deposits (the fields modified after Ye et al., 2011; Li et al., 2020).

6. Conclusions

(i) In-situ trace elements of sphalerite suggest that the resource endowments of critical metals in sphalerite are characterized by enrichment of Cd and Ge. Ge is mainly enriched in veined sphalerite (Sp-II) from the upper orebody with an elevation of > 180 m. The major critical metals incorporated into sphalerite are possibly controlled by the following substitutions: $Zn^{2+} \leftrightarrow Cd^{2+}$, $3Zn^{2+} \leftrightarrow 2\ Ga^{3+} + \square$, and $4Zn^{2+} \leftrightarrow Ge^{4+} + 2Fe^{2+} + \square$.

(ii) Calcite C-O isotopes indicates that the carbon originated from the dissolution of algal limestone in the Lower Cambrian Qingxudong Fm, whilst oxygen was likely derived from a binary mixing of wallrocks and basinal brine.

(iii) Calcite REE compositions indicate that REEs in the main ore-stage calcite were primarily sourced from the ore-host strata with additional contributions from the footwall sedimentary sequence and basal metamorphic rocks.

(iv) The deposit geology, calcite geochemistry, and trace element evidence in sphalerite suggest that the Danaopo was formed under a low-temperature and low f_{O2} reductive condition and is suitably classified as a Mississippi Valley-type deposit.

Declaration of Competing Interest

The authors declare that they have no known competing financial interests or personal relationships that could have appeared to influence the work reported in this paper.

Data availability

I have shared my data at the Atach file step

Acknowledgments

This study was supported by the National Natural Science Foundation of China (92162218 and 42202099), China Postdoctoral Science Foundation (2021M703190), Major Collaborative Innovation Projects for Prospecting Breakthrough Strategic Action of Guizhou Province, China ([2022] ZD004), and the Guizhou Provincial Natural Science Foundation (ZK[2023]477). We are grateful to the Editors and anonymous reviewers for their valuable feedback and comments.

Appendix A. Supplementary data

Supplementary data to this article can be found online at https://doi.org/10.1016/j.oregeorev.2023.105494.

References

Ao, S.F., Wang, Z.Q., Wang, C.Z., 2021. Analysis of the enriching behavior of associated and scattered germanium in the mineral processing of Huize lead-zinc mine. Min. Metall. 30, 25–31 in Chinese with English abstract.

Bau, M., 1991. Rare-earth element mobility during hydrothermal and metamorphic fluid-rock in traction and the significance of the oxidation state of europium. Chem. Geol. 93, 219–230.

Bau, M., Möller, P., 1995. Comparative study of yttrium and rare earth element behavior in fluorine−rich hydrothermal fluids. Contrib. Miner. Petrol. 119, 213–223.

Belissont, R., Boiron, M.C., Luais, B., Cathelineau, M., 2014. LA-ICP-MS analyses of minor and trace elements and bulk Ge isotopes in zoned Ge-rich sphalerites from the Noailhac SaintSalvy deposit (France): insights into incorporation mechanisms and ore deposition processes. Geochim. Cosmochim. Acta 126, 518–540.

Belissont, R., Muñoz, M., Boiron, M.C., Luais, B., Mathon, O., 2016. Distribution and oxidation state of Ge, Cu and Fe in sphalerite by μ-XRF and K-edge μ-XANES: insights into Ge incorporation, partitioning and isotopic fractionation. Geochim. Cosmochim. Acta 177, 298–314.

Bonnet, J., Mosser-Ruck, R., Caumon, M.-C., Rouer, O., Andre-Mayer, A.-S., Cauzid, J., Peiffert, C., 2016. Trace Element Distribution (Cu, Ga, Ge, Cd, and Fe) in Sphalerite from the Tennessee MVT Deposits, USA, By Combined EMPA, LA-ICP-MS, Raman Spectroscopy, and Crystallography. Can. Mineral. 54 (5), 1261–1284.

Bottinga, Y., 1968. Calculation of fractionation factors for carbon and oxygen isotopic exchange in the system calcite-carbon dioxide-water. J. Phys. Chem. 72 (3), 800–808.

Bradley, D.C., Leach, D.L., 2003. Tectonic controls of Mississippi Valley-type lead-zinc mineralization in orogenic forelands. Miner. Deposita 38 (6), 652–667.

Cai, Y.X., Yang, H.M., Duan, R.C., Lu, S.S., Zhang, L.G., Liu, Z.P., Qiu, X.F., 2014. Fluid inclusions and S, Pb, C isotope geochemistry of Pb-Zn deposits hosted by Lower

Cambrian in western Hunan-eastern Guizhou area. Geosci. 28, 29–41 in Chinese with English abstract.
Cao, L., Duan, Q.F., Peng, S.G., Zhou, Y., Li, K., Gan, J.M., 2017. Sources of metallogenic materials of lead-zinc deposits in western Hunan Province: Evidence from S and Pb isotopes. Geol. Bull. China 36, 834–845 in Chinese with English abstract.
Chen, L.u., Liu, Y., Hu, Z., Gao, S., Zong, K., Chen, H., 2011. Accurate determinations of fifty-four major and trace elements in carbonate by LA–ICP-MS using normalization strategy of bulk components as 100%. Chem. Geol. 284 (3-4), 283–295.
Chen, Y.P., Xiang, N., Tang, Q., Ma, C.C., 2018. Geological characteristics and metallogenic geological conditions of Danaopo Zn-Pb deposit in western Hunan. Miner. Explor. 9, 1127–1133 in Chinese with English abstract.
Cherniak, D.J., Zhang, X.Y., Wayne, N.K., Watson, E.B., 2001. Sr, Y and REE diffusion in fluorite. Chem. Geol. 181 (1-4), 99–111.
Cook, N.J., Ciobanu, C.L., Pring, A., Skinner, W., Shimizu, M., Danyushevsky, L., Saini-Eidukat, B., Melcher, F., 2009. Trace and minor elements in sphalerite: A LA-ICP-MS study. Geochim. Cosmochim. Acta 73 (16), 4761–4791.
Cook, N., Etschmann, B., Ciobanu, C., Geraki, K., Howard, D., Williams, T., Rae, N., Pring, A., Chen, G., Johannessen, B., Brugger, J., 2015. Distribution and substitution mechanism of Ge in a Ge-(Fe)-bearing sphalerite. Minerals 5 (2), 117–132.
Duan, Q.F., Cao, L., Zeng, J.K., Zhou, Y., Tang, Z.Y., Li, K., 2014. Rb-Sr dating of sphalerites from Shizishan Pb-Zn deposit and its geological significance in Huayuan Ore Concentration Area, Western Hunan. Earth Sci.-J. China Univ. Geosci. 39, 977–999 in Chinese with English abstract.
Frenzel, M., Hirsch, T., Gutzmer, J., 2016. Gallium, germanium, indium, and other trace and minor elements in sphalerite as a function of deposit type - A meta-analysis. Ore Geol. Rev. 76, 52–78.
Friedman, I., O'Neil, J.R., 1977. Compilation of stable isotope fractionation factors of geochemical interest. Data of Geochemistry. U.S. Geol. Surv. Prof. Pap. 440, 1–12.
Fu, S.Y., 2011. Discussion on the formation rules of high-grade Pb-Zn deposit in western Hunan Province. Nonferrous Met. Eng. 63, 27–35 in Chinese with English abstract.
Höll, R., Kling, M., Schroll, E., 2007. Metallogenesis of germanium—a review. Ore Geol. Rev. 30 (3–4), 145–180.
Hu, Y., Wei, C., Ye, L., Huang, Z., Danyushevsky, L., Wang, H., 2021. LA-ICP-MS sphalerite and galena trace element chemistry and mineralization-style fingerprinting for carbonate-hosted Pb-Zn deposits: Perspective from early Devonian Huodehong deposit in Yunnan. Ore Geol. Rev. 136, 104253.
Hu, P., Wu, Y., Zhang, C.Q., Hu, M.Y., 2014. Trace and minor elements in sphalerite from the Mayuan lead-zinc deposit, northern margin of the Yangtze Plate: implications from LA-ICP-MS analysis. Acta. Mineral. Sin. 34, 461–468 in Chinese with English abstract.
Hu, Y., Ye, L., Huang, Z., Wei, C., Wu, T., Xiang, Z., Liu, S., Li, Z., 2022. Genetic model for early Cambrian reef limestone-hosted Pb-Zn deposits in the world-class Huayuan orefield, South China: New insights from mineralogy, fluorite geochemistry and sulfides in situ S-Pb isotopes. Ore Geol. Rev. 141, 104682.
Huang, Z.L., Li, W.B., Chen, J., Xu, D.Y., Han, R.S., Liu, C.Q., 2010. REE and C-O isotopic geochemistry of calcites from world-class Huize Pb-Zn deposit, Yunnan, China: Implications for the ore genesis. Acta Geol. Sin. 84, 597–613.
Huston, D.L., Sie, S.H., Suter, G.F., Cooke, D.R., Both, R.A., 1995. Trace elements in sulfide minerals from Eastern Australian volcanic-hosted massive sulfide deposits: Part 1. Proton microprobe analyses of pyrite, chalcopyrite, and sphalerite, and Part 2. Selenium levels in pyrite: Comparison with d34S values and implications for the source of sulfur in volcanogenic hydrothermal systems. Econ. Geol. 90, 1167–1196.
Johan, Z., 1988. Indium and germanium in the structure of sphalerite: an example of coupled substitution with copper. Mineralogy and Petrology. 39, 211–229.
Kuang, W.L., Xiang, S.C., Xiao, W.Z., Chen, W., Yang, S.X., Yu, P.R., Chen, N.S., 2015. Metallogenic geological characteristics and genesis of lead-zinc deposits in northwestern Hunan. Miner. Deposita 34, 1072–1082 in Chinese with English abstract.
Kump, L.R., Arthur, M.A., 1999. Interpreting carbon-isotope excursions: carbonates and organic matter. Chem. Geol. 161 (1-3), 181–198.
Leach, D.L., Bradley, D.C., Huston, D., Pisarevsky, S.A., Taylor, R.D., Gardoll, S.J., 2010. Sediment-hosted lead-zinc deposits in earth history. Econ. Geol. 105 (3), 593–625.
Li, Z.F., 1992. S and Pb isotope from feature of Pb-Zn ore-belt in the border of GuizhouHunan Province, China. Geol. Guizhou 9 (3), 246–254 in Chinese with English abstract.
Li, K., Wu, C.X., Tang, C.Y., Duan, Q.F., Yu, Y.S., 2014. Carbon and oxygen isotopes of Pb-Zn ore deposits in western Hunan and eastern Guizhou Provinces and their implications for the ore-forming process. Geol. China 41, 1608–1619 in Chinese with English abstract.
Li, Z.L., Ye, L., Hu, Y.S., Wei, C., Huang, Z.L., Yang, Y.L., Danyushevsky, L., 2020. Trace elements in sulfides from the Maozu Pb-Zn deposit, Yunnan Province, China: implications for trace-element incorporation mechanisms and ore genesis. Am. Mineral. 1051, 1734–1751.
Li, B., Zhou, J.X., Huang, Z.L., Yan, Z.F., Bao, G.P., Sun, H.R., 2015. Geological, rare earth elemental and isotopic constraints on the origin of the Banbanqiao Zn-Pb deposit, Southwest China. J. Asian Earth Sci. 111, 100–112.
Liu, Y., Hu, Z., Gao, S., Günther, D., Xu, J., Gao, C., Chen, H., 2008. In situ analysis of major and trace elements of anhydrous minerals by LA-ICP-MS without applying an internal standard. Chem. Geol. 257 (1-2), 34–43.
Liu, Y.S., Hu, Z.C., Gao, S., Günther, D., Xu, J., Gao, C.G., Chen, H.H., 2010. Reappraisement and refinement of zircon U-Pb isotope and trace element analyses by LA-ICP-MS. Chin. Sci. Bull. 55 (15), 1535–1546.
Liu, H., Zhang, C.Q., Ji, X.J., Guo, Z.L., Lou, D.B., Wu, Y., Zhang, Y.F., Li, Y.L., 2022. Differential enrichment of germanium in sphalerite from Huize lead-zinc deposit, Yunnan Province. Mineral Deposits 41, 1057–1072 in Chinese with English abstract.
Liu, W.J., Zheng, R.C., 2000. Characteristics and movement of ore-forming fluids in the Huayuan lead-zinc deposit. Miner. Deposita 19, 173–181.
Luo, K., Zhou, J.-X., Huang, Z.-L., Wang, X.-C., Wilde, S.A., Zhou, W., Tian, L., 2019. New insights into the origin of early Cambrian carbonate-hosted Pb-Zn deposits in South China: a case study of the Maliping Pb-Zn deposit. Gondw. Res. 70, 88–103.
Luo, K., Zhou, J.X., Huang, Z.L., Caulfield, J., Zhao, J.X., Feng, Y.X., Ouyang, H., 2020. New insights into the evolution of Mississippi Valley-Type hydrothermal system: a case study of the Wusihe Pb-Zn deposit, South China, using quartz in-situ trace elements and sulfides in situ S-Pb isotopes. Am. Miner. 105 (1), 35–51.
Luo, K., Cugerone, A., Zhou, M.-F., Zhou, J.-X., Sun, G.-T., Xu, J., He, K.-J., Lu, M.-D., 2022. Germanium enrichment in sphalerite with acicular and euhedral textures: an example from the Zhulingou carbonate-hosted Zn(-Ge) deposit, South China. Miner. Deposita 57 (8), 1343–1365.
Luo, W., Yin, Z., Kong, L., Dai, T.G., 2009. Discussion on the geological features and genesis of the Limei Pb-Zn ore concentration belt in northwestern Hunan Province. Geol. Surv. Res. 33, 194–202 in Chinese with English abstract.
Mao, D.L., 2016. Geological characteristics and genesis of the Danaopo Zn-Pb deposit in Huayuan County, Hunan Province. Modern Mining 562, 90–97 in Chinese with English abstract.
Michard, A., 1989. Rare earth element systematics in hydrothermal fluids. Geochim. Cosmochim. Acta 53 (3), 745–750.
Möller, P., 1987. Correlation of homogenization temperatures of accessory minerals from sphalerite-bearing deposits and Ga/Ge model temperatures. Chem. Geol. 61, 153–159.
Ohmoto, H., 1986. Stable isotope geochemistry of ore deposits. Rev. Mineral. 16, 491–560.
Ohr, M., Halliday, A.N., Peacor, D.R., 1994. Mobility and fractionation of rare earth element in argillaceous sediments: implications for dating diagenesis and low-grade metamorphism. Geochim. Cosmochim. Acta 58, 289–312.
O'Neil, J.R., Clayton, R.N., Mayeda, T.K., 1969. Oxygen isotope fractionation in divalent metal carbonates. J. Chem. Phys. 51 (12), 5547–5558.
Oyebamiji, A., Hu, R.Z., Zhao, C.H., Zafar, T., 2020. Origin of the Triassic Qilinchang Pb-Zn deposit in the western Yangtze Block, SW China: Insights from in-situ trace elemental compositions of base metal sulphides. J. Asian Earth Sci. 192, 104292.
Schneider, J., Boni, M., Lapponi, F., Bechstadt, T., 2002. Carbonate-hosted zinc-lead deposits in the Lower Cambrian of Hunan, South China: a radiogenic (Pb, Sr) isotope study. Econ. Geol. 97 (8), 1815–1827.
Schönenberger, J., Köhler, J., Markl, G., 2008. REE systematics of fluorides, calcite and siderite in peralkaline plutonic rocks from the Gardar Province, South Greenland. Chem. Geol. 247 (1-2), 16–35.
Souissi, F., Jemmali, N., Souissi, R., Dandurand., 2013. REE and isotope (Sr, S and Pb) geochemistry to constrain the genesis and timing of the F-(Ba-Pb-Zn) ores of the Zaghouan District (NE Tunisia). Ore Geology Reviews, 55, 1–12.
Sverjensky, D.A., 1984. Europium redox equilibria in aqueous solution. Earth Planet. Sci. Lett. 67 (1), 70–78.
Tan, J.J., Liu, C.P., Yang, H.M., Cai, Y.X., Lu, S.S., 2018. Geochronology and ore-forming material source constraints for Rouxianshan Pb-Zn deposit in Huayuan ore concentration area, western Hunan. Earth Sci. 43 (7), 2438–2448 in Chinese with English abstract.
Taylor, H.P., Frechen, J., Degens, E.T., 1967. Oxygen and carbon isotope studies of carbonatites from the Laacher See District, West Germany and the Alnö District, Sweden. Geochimica et Cosmochimica Acta. 31 (3), 407–430.
Veizer, J., Hoefs, J., 1976. The nature of $^{18}O/^{16}O$ and $^{13}C/^{12}C$ secular trends in sedimentary carbonate rocks. Geochim. Cosmochim. Acta 40, 1387–1395.
Wang, X.L., Zhou, J.C., Qiu, J.S., Jiang, S.Y., Shi, Y.R., 2008. Geochronology and geochemistry of Neoproterozoic mafic rocks from western Hunan, South China: implications for petrogenesis and post-orogenic extension. Geol. Mag. 145, 215–233.
Wei, H.T., 2017. Mineralization of the Huayuan Pb-Zn orefield, western Hunan (PH.D, thesis). Central South University, pp. 7–9. in Chinese with English abstract.
Wei, C., Ye, L., Hu, Y., Danyushevskiy, L., Li, Z., Huang, Z., 2019. Distribution and occurrence of Ge and related trace elements in sphalerite from the Lehong carbonate-hosted Zn-Pb deposit, northeastern Yunnan. Ore Geol. Rev. 115, 103175.
Wei, C., Ye, L., Hu, Y., Huang, Z., Danyushevsky, L., Wang, H., 2021a. LA-ICP-MS analyses of trace elements in base metal sulfides from carbonate-hosted Zn-Pb deposits, South China: a case study of the Maoping deposit. Ore Geol. Rev. 130, 103945.
Wei, C., Huang, Z., Ye, L., Hu, Y., Santosh, M., Wu, T., He, L., Zhang, J., He, Z., Xiang, Z., Chen, D.a., Zhu, C., Jin, Z., 2021b. Genesis of carbonate-hosted Zn-Pb deposits in the Late Indosinian thrust and fold systems: An example of the newly discovered giant Zhugongtang deposit, South China. J. Asian Earth Sci. 220, 104914.
Wei, H.T., Shao, Y.J., Ye, Z., Xiong, Y.Q., Zhou, H.D., Xie, Y.L., 2017. REE and Sr isotope geochemistry of gangue calcites from Huayuan Pb-Zn orefield in western Hunan, China. Chin. J. Nonferrous Metals 27, 2329–2336 in Chinese with English abstract.
Wei, H.T., Shao, Y.J., Xiao, K.Y., Kong, H., Zhang, S., Wang, K., Li, Q., Chen, B.H., Xiang, J., Wen, C.H., 2020. Modeling-based mineral system approach to prospectivity mapping of stratabound hydrothermal deposits: A case study of MVT Pb-Zn deposits in the Huayuan area, northwestern Hunan Province, China. Ore Geol. Rev. 120, 1–12.
Wei, H.T., Shao, Y.J., Ye, Z., Zhou, H.D., 2021c. Geochemical characteristics of trace elements of sphalerite from Huayuan Pb-Zn ore field, western Hunan, China. J. Chengdu Univ. Technol. 48, 142–153 in Chinese with English abstract.
Wood, S.A., Samson, I.M., 2006. The aqueous geochemistry of gallium, germanium, indium and scandium. Ore Geol. Rev. 28 (1), 57–102.
Wu, T., Huang, Z.L., Xiang, Z.Z., Ye, L., Sui, Z.H., Hu, Y.S., Yan, Z.F., 2020. In situ trace element study of pyrites from the Danaopo super-large Pb-Zn deposit in the western

Hunan, China. Acta Mineralogica Sinica. 40, 430–440 in Chinese with English abstract.
Wu, T., Huang, Z., Ye, L., Wei, C., Chen, J., Yang, M., Yan, Z., Sui, Z., 2021. Origin of the carbonate-hosted Danaopo Zn-Pb deposit in western Hunan Province, China: Geology and in-situ mineral S-Pb isotope constraints. Ore Geol. Rev. 129, 103941.
Xia, X.J., Shu, J.W., 1995. Geological characteristics and genesis of the Limei zinc Deposit. Geotecton. Metallog. 19, 197–204. In Chinese.
Xiong, Y., 2007. Hydrothermal thallium mineralization up to 300 °C a thermodynamic approach. Ore Geol. Rev. 32, 291–313.
Yang, S.X., Lao, K.T., 2007. Geological characteristics and ore indicators of lead-zinc deposits in northwestern Hunan, China. Geol. Bull. China 26, 899–908 in Chinese with English abstract.
Yao, W.H., Li, Z.X., 2016. Tectonostratigraphic history of the Ediacaran-Silurian Nanhua foreland basin in South China. Tectonophysics 674, 31–51.
Ye, L., Cook, N.J., Ciobanu, C.L., Liu, Y.P., Zhang, Q., Liu, T.G., Gao, W., Yang, Y.L., Danyushevskiy., L., 2011. Trace and minor elements in sphalerite from base metal deposits in South China: A LA-ICPMS study. Ore Geology Reviews, 39, 188–217.
Ye, L., Li, Z.L., Hu, Y.S., Huang, Z.L., Zhou, J.X., Fan, H.F., Danyushevsky, L., 2016. Trace elements in sulfide from the Tianbaoshan Pb-Zn deposit, Sichuan Province, China: A LA-ICPMS study. Acta Petrol. Sin. 32 (11), 3377–3393 in Chinese with English abstract.
Yu, P.R., Deng, W.D., Zeng, J.K., Mao, D.L., 2014. The general survey report of Danaopo Zn-Pb deposit in Huayuan orefield, western Hunan Province. Team of Hunan Geol. Miner. Bureau 5–119. Unpub. Report. 405(in Chinese.
Yuan, B., Zhang, C.Q., Yu, H.J., Yang, Y.M., Zhao, Y.X., Zhu, C.C., Ding, Q.F., Zhou, Y.B., Yang, J.C., Xu, Y., 2018. Element enrichment characteristics: Insights from element geochemistry of sphalerite in Daliangzi Pb-Zn deposit, Sichuan, Southwest China. J. Geochem. Explor. 186, 187–201.
Zhang, C.H., Gao, L.Z., Shi, X.Y., Han, Y., Liu, Y.M., 2014. SHRIMP age of the volcanic rock from the Fanjingshan Group and its chronostratigraphic significance. Earth Sci. Front. 21, 139–143 in Chinese with English abstract.
Zheng, Y.-F., 1999. Oxygen isotope fractionation in carbonate and sulfate minerals. Geochem. J. 33 (2), 109–126.
Zheng, Y.F., Hoefs, J., 1993. Carbon and oxygen isotopic covariations in hydrothermal calcites. Miner. Deposita 28, 79–89.
Zheng, M.H., Wang, X.C., 1991. Ore genesis of the Daliangzi Pb-Zn deposit in Sichuan, China. Econ. Geol. 86, 831–846.
Zhou, Y., Duan, Q.F., Tang, J.X., Cao, L., Li, F., Huang, H.Q., Gan, J.M., 2014. The large-scale low-temperature mineralization of lead-zinc deposits in western Hunan: Evidence from fluid inclusions. Geol. Explor. 50, 515–532 in Chinese with English abstract.
Zhou, Y., Duan, Q.F., Chen, Y.C., Tang, J.X., Cao, L., Peng, S.G., Gan, J.M., 2017. C, O, H, S, Pb and Sr isotope constraints on the metals sources of Huayuan Pb-Zn deposit in western Hunan Province. Acta Geol. Sin. 90, 2786–2802 in Chinese with English abstract.
Zhou, Y., Duan, Q.F., Cao, L., Yu, Y.S., Gan, J.M., 2021. Rb-Sr dating and ore-forming material tracing of sphalerite from Limei Pb-Zn deposit in Huyuan ore concentration are of Hunan, China. J. Earth Sci. Environ. 43, 661–673 in Chinese with English abstract.
Zhou, J.X., Huang, Z.L., Yan, Z.F., 2013. The origin of the Maozu carbonate-hosted Pb-Zn deposit, southwest China: constrained by C-O-S-Pb isotopic compositions and Sm-Nd isotopic age. J. Asian Earth Sci. 73, 39–47.
Zhou, J.X., Wang, X.C., Wilde, S.A., Luo, K., Huang, Z.L., Wu, T., Jin, Z.G., 2018a. New insights into the metallogeny of MVT Pb-Zn deposits: A case study from the Nayongzhi in South China, using field data, fluid compositions, and in situ S-Pb isotopes. Am. Mineral. 103, 91–108.
Zhou, J.X., Luo, K., Wang, X.C., Wilde, S.A., Wu, T., Huang, Z.L., Cui, Y.L., Zhao, J.X., 2018b. Ore genesis of the Fule Pb-Zn deposit and its relationship with the Emeishan Large Igneous Province: evidence from mineralogy, bulk C-O-S and in situ S-Pb isotopes. Gondw. Res. 54, 161–179.
Zhou, J.X., Xiang, Z.Z., Zhou, M.F., Feng, Y.X., Luo, K., Huang, Z.L., Wu, T., 2018c. The giant Upper Yangtze Pb-Zn province in SW China: Reviews, new advances and a new genetic model. J. Asian Earth Sci. 2018 (154), 280–315.
Zhou, J.X., Yang, Z.M., An, Y.L., Luo, K., Liu, C.X., Ju, Y.W., 2022. An evolving MVT hydrothermal system: Insights from the Niujiaotang Cd-Zn ore field, SW China. J. Asian Earth Sci. 2022 (237), 105357.
Zhuang, L.L., Song, Y.C., Liu, Y.C., Fard, M., Hou, Z.Q., 2019. Major and trace elements and sulfur isotopes in two stages of sphalerite from the world-class Angouran Zn–Pb deposit, Iran: Implications for mineralization conditions and type. Ore Geol. Rev. 109, 184–200.
Zou, Z.C., Hu, R.Z., Bi, X.W., Ye, L., Wu, L.Y., Peng, C.X., Tang, Y.Y., 2012. Trace element geochemistry of the Liziping Pb-Zn deposit, the Lanping Basin, Northwest Yunnan Province, China. Geochimica 41, 482–496 in Chinese with English abstract.